Structures of the Hexafluorocyclopropane, Octafluorocyclobutane, and Decafluorocyclopentane Radical Anions Probed by Experimental and Computational Studies of Anisotropic Electron Spin Resonance (ESR) Spectra

Masaru Shiotani*

Department of Applied Chemistry, Graduate School of Engineering, Hiroshima University, Higashi−Hiroshima 739-8527, Japan

Anders Lund

Department of Physics, Chemistry and Biology, Linköping University, S-581 83 Linköping, Sweden

Sten Lunell

Department of Quantum Chemistry, Uppsala University, S-751 20 Uppsala, Sweden

Ffrancon Williams

Department of Chemistry, University of Tennessee, Knoxville, Tennessee 37996-1600

Received: July 31, 2006; In Final Form: October 21, 2006

Anisotropic electron spin resonance (ESR) spectra are reported for the radical anions of hexafluorocyclopropane (c-$C_3F_6^-$), octafluorocyclobutane (c-$C_4F_8^-$), and decafluorocyclopentane (c-$C_5F_{10}^-$) generated via γ-irradiation in plastically crystalline tetramethylsilane (TMS) and rigid 2-methyltetrahydrofuran (MTHF) matrices. By combining the analysis of these experimental ESR spectra involving anisotropic hyperfine (*hf*) couplings with a series of quantum chemical computations, the geometrical and electronic structure of these unusual perfluorocycloalkane radical anions have been characterized more fully than in previous studies that considered only the isotropic couplings. Unrestricted Hartree-Fock (UHF) computations with the 6-311+G(d,p) basis set predict planar ring structures for all three radical anions, the ground electronic states being $^2A_2''$ for c-$C_3F_6^-$ (D_{3h} symmetry), $^2A_{2u}$ for c-$C_4F_8^-$ (D_{4h}), and $^2A_2''$ for c-$C_5F_{10}^-$ (D_{5h}), in which the respective six, eight, and ten ^{19}F-atoms are equivalent by symmetry. A successful test of the theoretical computation is indicated by the fact that the isotropic ^{19}F *hf* couplings computed by the B3LYP method with the 6-311+G-(2df,p) basis set for the optimized geometries are in almost perfect agreement with the experimental values: viz., 19.8 mT (exp) vs 19.78 mT (calc) for c-$C_3F_6^-$; 14.85 mT (exp) vs 14.84 mT (calc) for c-$C_4F_8^-$; 11.6 mT (exp) vs 11.65 mT (calc) for c-$C_5F_{10}^-$. Consequently, the same computation method has been applied to calculate the almost axially symmetric anisotropic ^{19}F *hf* couplings for the magnetically equivalent ^{19}F atoms: (−4.90 mT, −4.84 mT, 9.75 mT) for c-$C_3F_6^-$, (−3.54 mT, −3.48 mT, 7.02 mT) for c-$C_4F_8^-$, and (−2.62 mT, −2.56 mT, 5.18 mT) for c-$C_5F_{10}^-$. ESR spectral simulations performed using the computed principal values of the *hf* couplings and the spatial orientations of the ^{19}F nuclei as input parameters reveal an excellent fit to the experimental anisotropic ESR spectra of c-$C_3F_6^-$, c-$C_4F_8^-$, and c-$C_5F_{10}^-$, thereby providing a convincing proof of the highly symmetric D_{nh} structures that are predicted for these negative ions. Furthermore, using the computed ^{19}F principal values and their orientations, the effective ^{19}F anisotropic *hf* couplings along the molecular symmetry axes were evaluated for c-$C_3F_6^-$ and c-$C_4F_8^-$ and successfully correlated with the positions of the characteristic outermost features in both the experimental and calculated anisotropic spectra. In addition, the electronic excitation energies and oscillator strengths for the c-$C_3F_6^-$, c-$C_4F_8^-$, and c-$C_5F_{10}^-$ radical anions were computed for the first time using time-dependent density functional theory (TD-DFT) methods.

1. Introduction

Interest in the structure and stability of perfluorocycloalkane negative ions comes from both the unusual nature of these species and their significant role in numerous applications of the parent compounds. Thus, perfluorocyclobutane (c-C_4F_8) gas is widely used both as a feedstock for ion plasmas used in the etching and fabrication of microelectronic components,[1,2] and as a suitable dielectric in high-voltage insulators.[3] Because perfluorocycloalkanes (c-C_nF_{2n}) are saturated molecules, it is generally considered surprising that they should form stable negative ions,[4] given that a process in which a single C−F bond functions as an electron-accepting group would most likely result in dissociation to a perfluorocycloalkyl radical and a fluoride anion. Indeed, studies by cyclic voltammetry indicate that such

* Author to whom correspondence should be addressed. E-mail address: mshiota@hiroshima-u.ac.jp.

10.1021/jp064891u CCC: $37.00
Published on Web 12/22/2006

component reactions occur in the electrochemical reduction of perfluorodecalin and other saturated perfluorocarbons.[5] Moreover, this general mechanism of dissociative electron transfer is well-known to occur for many saturated halogen-containing compounds, such as the alkyl halides.[6]

Therefore, the detailed molecular and electronic characterization of perfluorocycloalkane negative ions (c-$C_nF_{2n}^-$) represents a significant challenge to both the experimental work and the underlying theory, the main problem being to connect quantum chemical calculations with diagnostic spectroscopic information on the structure. However, gas-phase studies have had a tendency to concentrate largely on the determination of cross sections for electron attachment at different electron energies,[7] which are processes that do not directly relate to the structure of the negative ion in the ground state. Also, there has hitherto been no complete spectroscopic study of photodetachment transitions for the widely studied c-$C_4F_8^-$ ion in the gas phase,[4,8] and the published experimental determinations of the adiabatic electron affinity rely largely on the macroscopic thermodynamic approach implicit in the use of van't Hoff plots of the logarithm of the rate constant for electron detachment versus $1/T$.[9−11] Although recent computational estimates of the adiabatic electron affinity[4,12,13] certainly provide a suitable check on these experimental values, such agreement adds little in the way of discriminating between fine points of structure at the molecular level.

In contrast to the limitations of gas-phase investigations, matrix-isolation electron spin resonance (ESR) studies at low temperatures can provide direct information on the molecular structure of these negative ion species through determinations of the ^{19}F and ^{13}C hyperfine (*hf*) coupling (or splitting) constants.[13,15,16] These spectroscopic parameters now can also be predicted with considerable precision by recent advances in computational methods involving density functional theory (DFT),[13,14] thereby affording a valuable bridge between experiment and theory at a most fundamental level. Previous work[13,15,16] has focused largely on the *isotropic* coupling constants and, in particular, has established the equivalence of all the $2n$ fluorines in each of these c-$C_nF_{2n}^-$ ($n = 3-5$) negative ions. Furthermore, the sum of the isotropic ^{19}F coupling constants for each species remains essentially constant along the series for $n = 3-5$, indicating a delocalization of the unpaired electron over the entire molecule.[13,15,16] In the most-recent study,[13] the finding of a small isotropic ^{13}C *hf* coupling for the c-$C_4F_8^-$ ion has provided evidence for a π-like (rather than a σ-like) delocalized singly occupied molecular orbital (SOMO) in a D_{4h} structure, which has a nodal plane that occurs at the carbon ring that forms the σ_h symmetry element. This a_{2u} orbital is C−C bonding and C−F antibonding, with the wavefunction amplitude being uniformly distributed over C−C π and C−F σ^* orbitals.[13]

Despite these successes based on the experimental analysis and theoretical calculation of isotropic ESR *hf* couplings, a more-stringent test of perfluorocycloalkane negative-ion structure is afforded by a thorough examination of the anisotropic parameters, because these quantities are tensors that involve both magnitude and direction. Therefore, these parameters provide a particularly sensitive gauge of both geometrical and electronic structure, and, hence, the rigid-limit ESR spectra should be highly responsive to any deviations from the high molecular symmetries that are predicted by the quantum chemical calculations.[4,12,13] Moreover, at least in principle, a clear distinction between fluxional and single-minimum structures can be sought at low temperatures through anisotropic ESR spectral measurements, and the present paper reports a comprehensive experimental and computational study along these lines. Previous work has been limited to a single report on the ESR powder spectrum of c-$C_4F_8^-$;[17] however, no analysis of the complicated pattern was attempted, with the c-$C_4F_8^-$ spectrum in this case being used simply as a convenient analytical fingerprint to show that the tetrafluoroethylene radical anion ($C_2F_4^-$) undergoes a bimolecular reaction with neutral C_2F_4 on matrix annealing to generate c-$C_4F_8^-$.[13,17,18]

2. Experimental and Computational Methods

2.1. Materials. A sample of hexafluorocyclopropane (c-C_3F_6) was kindly donated to us by Dr. R. W. Fessenden from material that was originally prepared by Dr. K. Harman. Octafluorocyclobutane (c-C_4F_8) was obtained from Peninsular Chemical Research (PCR, Inc.) and from Air Products and Chemicals, Inc.; decafluorocyclopentane (c-C_5F_{10}) was obtained from PCR, Inc.; neopentane (Neop: $C(CH_3)_4$) was obtained from Matheson Gas Products; tetramethylsilane (TMS, $Si(CH_3)_4$) was obtained from either Mallinckrodt or the Norell Chemical Co.; tetramethylsilane-d_{12} (TMS-d_{12}, $Si(CD_3)_4$) was obtained from Merck, Sharp and Dohme Ltd.; and 2-methyltetrahydrofuran (MTHF) was obtained from Eastman Organic Chemicals.

2.2. ESR Samples and Measurements. The perfluorocycloalkane radical anions were generated by γ-ray irradiation at 77 K of solid solutions containing ca. 1 mol % of the perfluorocycloalkane in the solid Neop, TMS, TMS-d_{12} or MTHF matrix.[13−18] ESR measurements were conducted at variable temperatures in the range of 77−170 K using the Varian (model V-4502-15) or JEOL (model JES-RE1X) X-band spectrometers operating at 100 kHz modulation.[13,14] The photobleaching experiments were performed using unfiltered light from a tungsten lamp. The large ^{19}F *hf* splittings were calculated from the spectral line positions using the higher-order solutions[19−21] of the appropriate spin Hamiltonian.

2.3. Computations. Quantum chemical computations were performed to compare the ESR ^{13}C and ^{19}F *hf* splittings with the experimental ones and to provide information on the electronic structures of the radical anions. The Gaussian 03 suite of programs were used for quantum chemical computations, and the abbreviations relating to the computations are taken from this program package.[22] The B3LYP, MP2, and UHF methods were used for geometry optimizations with the 6-31+G(d,p) and 6-311+G(d,p) basis sets. Furthermore, both the B3LYP and MP2 methods were used to compute the ESR *hf* splittings with the 6-31+G(2df,p) and 6-311+G(2df,p) basis sets for the optimized structures. Excitation energies and oscillator strengths of the radical anions were computed by the TD (time-dependent) B3LYP methods with the 6-311+G(d,p) basis set. For "powder" ESR spectral simulations of amorphous samples involving anisotropic *hf* couplings (or splittings), which are briefly referenced as "powder" or "anisotropic" samples in the following, the homemade program "Xfit" was applied.[23,24] As is known, partly by our own previous work,[25] the directions of the principal axes of the anisotropic ^{19}F *hf* couplings are usually not collinear with or perpendicular to the C−F bonds, but must be theoretically computed, in this work by code implemented in Gaussian 03.[22]

3. Results and Discussion

3.1. Variable-Temperature ESR Spectra. Previous papers[13,15,16] have reported the isotropic ESR spectra of the c-$C_3F_6^-$, c-$C_4F_8^-$, and c-$C_5F_{10}^-$ radical anions generated and stabilized in the neopentane, TMS, and hexamethylethane

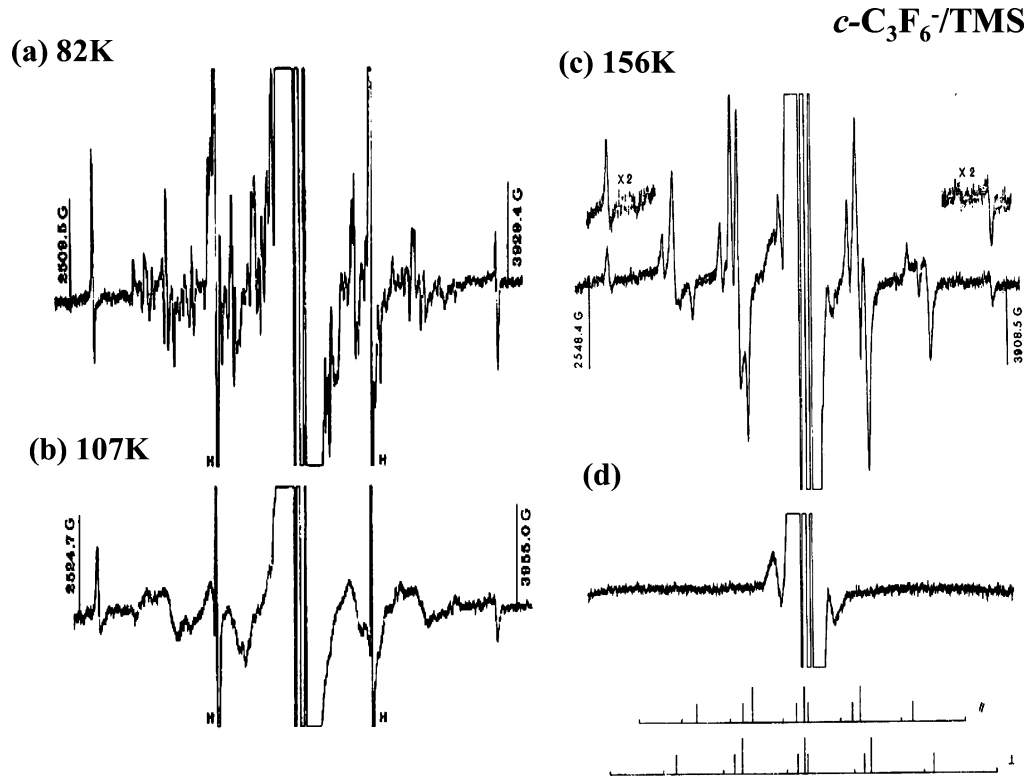

Figure 1. Temperature-dependent electron spin resonance (ESR) spectra of c-$C_3F_6^-$ (ν = 9117.5 Hz) generated by γ-ray irradiation of the solid solution of 1 mol % c-C_3F_6 in tetramethylsilane (TMS) at 77 K: (a) 82 K, (b) 107 K, and (c) 156 K. The spectra were recorded at the same amplifier gain. Spectrum (d) was recorded at 156 K after exposing the sample to unfiltered light from a tungsten lamp, and the line diagram at the bottom of this panel shows the expected positions of the second-order ^{19}F hyperfine (*hf*) lines calculated from the parameters listed in Table 1 for the c-$C_3F_6^-$ radical anion. (10 G = 1 mT, where G represents Gauss.)

TABLE 1: Experimental ^{19}F and ^{13}C Isotropic Hyperfine (*hf*) Splittings and *g*-Values for Perfluorocycloalkane Radical Anions, c-$C_nF_{2n}^-$ (n = 3, 4, 5), from Various Matrix Electron Spin Resonance (ESR) Studies

radical anion	matrix[a]	T (K)	g value[b]	$a(^{19}F)$ and $a(^{13}C)$ (mT)[c]	note
c-$C_3F_6^-$	Neop	125	2.0031	19.8 (for six ^{19}F)	present work (and ref 16)
c-$C_3F_6^-$	TMS	147	2.0028[d] ($g_\parallel$ = 2.0040, $g_\perp$ = 2.0022)	19.8[d] ($A_\parallel$ = 17.6, $A_\perp$ = 20.8) (for six ^{19}F)	present work (and ref 16)
c-$C_3F_6^-$	HME	160	2.0027 ± 0.0006	19.86 (for six ^{19}F)	ref 13
c-$C_4F_8^-$	Neop	130	2.0021	14.8 (for eight ^{19}F)	present work (and refs 15 and 16)
c-$C_4F_8^-$	TMS	113	2.0022[d] ($g_\parallel$ = 2.0023, $g_\perp$ = 2.0022)	14.85[d] ($A_\parallel$ = 14.45, $A_\perp$ = 15.05) (for eight ^{19}F)	present work
c-$C_4F_8^-$	HME	163	2.0021	14.84 (for eight ^{19}F)	ref 13
c-$C_4F_8^-$	HME	163		0.52 (for four ^{13}C)	ref 13
c-$C_5F_{10}^-$	Neop	127	2.0028	11.7 ± 0.1 (for ten ^{19}F)	present work
c-$C_5F_{10}^-$	TMS	167	2.0031[d] ($g_\parallel$ = 2.0027, $g_\perp$ = 2.0034)	11.6[d] ($A_\parallel$ = 12.2, $A_\perp$ = 11.3) (for ten ^{19}F)	present work
c-$C_5F_{10}^-$	HME	165	2.0027	11.79 (for ten ^{19}F)	ref 13

[a] Neop = neopentane ($C(Me)_4$), TMS = tetramethylsilane ($Si(Me)_4$), and HME = hexamethylethane ($C_2(Me)_6$). [b] Error limits are estimated to be ±0.0006, except for c-$C_4F_8^-$ in HME (±0.0008). [c] Error limits are ±0.1 and ±0.04 mT for the c-$C_nF_{2n}^-$ (n = 3, 4, 5) in Neop and TMS, and HME, respectively, except for c-$C_4F_8^-$ in TMS (±0.05 mT).[13,15,16] [d] The isotropic value was determined by averaging the measured parameters for a spectrum showing residual anisotropy.

(HME) matrices. The present work extends the matrix-isolation studies of these negative-ion species to consider the temperature-dependent ESR spectra, which reveal the presence of anisotropic features. [It should, of course, be understood that the common shorthand use of the term "anisotropic ESR spectra" in this paper refers, strictly speaking, to ESR spectra involving anisotropic *hf* couplings.] A detailed analysis of these spectra leads to the determination of anisotropic spectral parameters, from which the isotropic *hf* couplings are derived. The results obtained for each of these radical anions in the different matrices are briefly described and summarized. In this section, we concentrate mainly on the ESR spectra that involve anisotropic couplings observed in the TMS matrix.

3.1.1. Hexafluorocyclopropane Radical Anion (c-$C_3F_6^-$). Figure 1 shows the ESR spectra of c-$C_3F_6^-$ in the TMS matrix measured in the temperature range of 82−156 K. Spectrum (c), recorded at 156 K, is almost isotropic in appearance but, after closer analysis, is observed to retain a definite residual anisotropy. The spectrum can be analyzed in terms of a radical that possesses six equivalent ^{19}F nuclei; the line diagram shows parallel and perpendicular components with the expected positions of the second-order *hf* lines[20,26,27] calculated from $A_\parallel$ (six ^{19}F) = 17.6 mT and $A_\perp$ (six ^{19}F) = 20.8 mT (see Table 1). The axially symmetric ^{19}F *hf* splittings and *g*-values suggest that (i) a rapid reorientation of c-$C_3F_6^-$ occurs about an effective molecular axis in the matrix, and (ii) this motion also confers directional equivalence on all six fluorines. For example, a rotation about the major C_3 axis perpendicular to the σ_h plane of the D_{3h} point group would render all of the fluorines equivalent in cylindrical symmetry, while each still retains

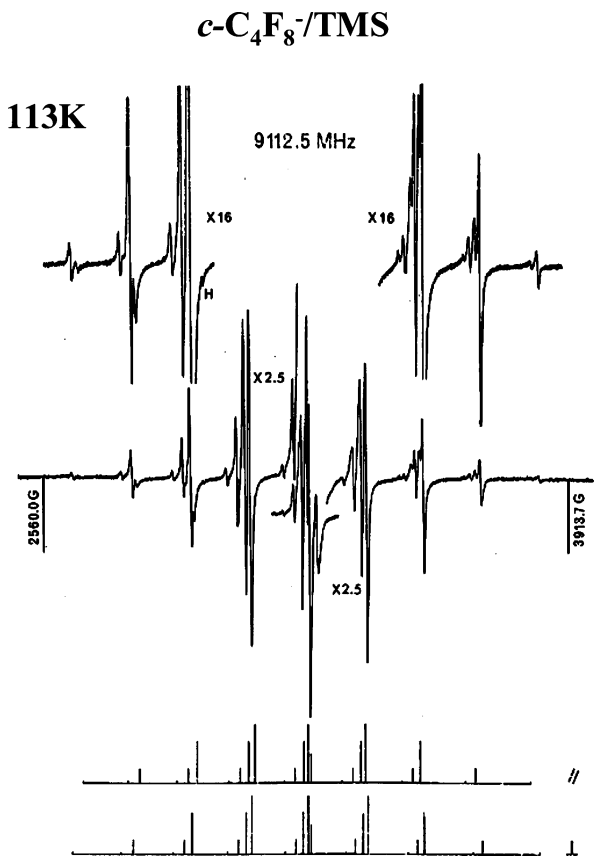

Figure 2. ESR spectrum of c-$C_4F_8^-$ recorded at 113 K (ν = 9112.5 Hz). The c-$C_4F_8^-$ radical was generated by γ-ray irradiation of the solid solution of 1 mol % c-C_4F_8 in TMS at 77 K. The line diagram at the bottom of this panel shows the expected positions of the second-order ^{19}F *hf* lines calculated from the parameters listed in Table 1 for the c-$C_4F_8^-$ radical anion. (10 G = 1 mT.)

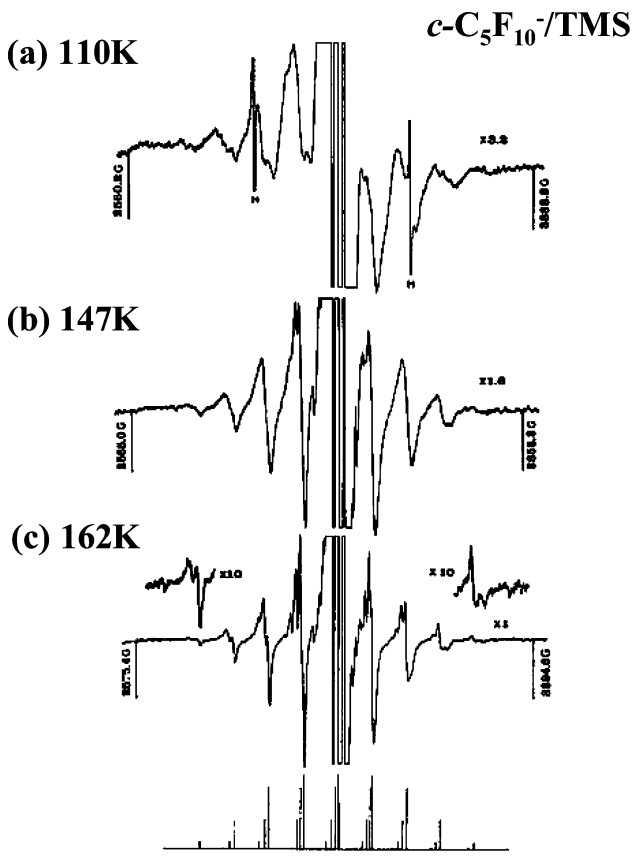

Figure 3. Temperature-dependent ESR spectra of c-$C_5F_{10}^-$ (ν = 9117.5 Hz) generated by γ-ray irradiation of the solid solution of 1 mol % c-C_5F_{10} in TMS at 77 K: (a) 110 K, (b) 147 K, and (c) 162 K. The line diagram at the bottom of the figure shows the expected positions of the second-order ^{19}F *hf* lines calculated from the parameters listed in Table 1 for the c-$C_5F_{10}^-$ radical anion. (10 G = 1 mT.)

significant individual ^{19}F *hf* anisotropy. The isotropic ^{19}F *hf* splitting, calculated from $^1/_3(A_{||} + 2A_\perp)$, is 19.8 mT (see Table 1).

After the sample is cooled from 156 K to *ca*. 110 K, the spectral lines become broader, as can be seen in spectrum (b). At the same time, the lines move outward, to give a larger total splitting. Thus, the separation between the two outermost lines, which consist of the $M_I = \pm 3$ perpendicular features, where M_I represents the *z*-component of the total nuclear spin state (I) of the six equivalent ^{19}F ($I = ^1/_2$) nuclei, increases from 124.5 mT (156 K) to 130.2 mT (107 K). After further decreasing the temperature to ca. 80 K, these outermost lines move still further apart and, concomitantly, the entire spectrum changes to a much more complicated *hf* structure with many lines and a narrower line width, as can be seen in spectrum (a), where the total spectral width has now increased to 132.7 mT (82 K). This spectral change upon cooling can be reasonably attributed to the transition from the almost isotropic to the anisotropic spectrum. The spectrum at 82 K can, in fact, be successfully interpreted as that expected in the rigid limit. This is accomplished by means of a spectral simulation, using the computed principal values and directions of the ^{19}F *hf* splitting tensors, as will be mentioned later in section 3.3, "ESR Spectra Involving Anisotropic Couplings: Comparison of Experimental and Computational Results".

3.1.2. Octafluorocyclobutane Radical Anion (c-$C_4F_8^-$). Figure 2 shows the ESR spectrum of c-$C_4F_8^-$ in TMS recorded at 113 K, with the well-defined ^{19}F *hf* pattern lying outside the intense central band that results from the background radicals derived from the matrix. As with c-$C_3F_6^-$, the spectrum is almost isotropic but, after closer examination, shows some residual anisotropy. The spectrum can be analyzed in terms of a radical that possesses eight equivalent ^{19}F nuclei, as described in previous reports.[15,16] Although the spectral resolution is slightly inferior to that of c-$C_4F_8^-$ in HME recorded at 163 K,[13] all of the second-order *hf* lines[20,26,27] expected for the eight equivalent ^{19}F nuclei are well-resolved. The line diagram in Figure 2 shows the parallel and perpendicular components that correspond to the expected positions of the second-order *hf* patterns calculated from $A_{||}$ = 14.45 mT and $A_\perp$ = 15.05 mT; the derived isotropic ^{19}F *hf* splitting is 14.85 mT (see Table 1).

After the sample was cooled from 113 K to 80 K, the spectral resolution gradually deteriorated, because of line broadening. However, the original isotropic character of the spectrum persisted, even at 80 K, without any indication of a gradual transition to an anisotropic pattern. Moreover, increasing the temperature from 113 K to 130 K provided no significant improvement in the spectral resolution, as shown in the previous paper (see Figure 1 in ref 16). Thus, the combination of c-C_4F_8 as the solute and TMS as the matrix seems to be quite unique, insofar as it is suitable for observing the highly resolved isotropic ESR spectrum of the radical anion, but is unsuitable for observing its anisotropic spectrum. Hence, we applied the MTHF matrix, instead of TMS, to observe a fully anisotropic spectrum. This rigid-limit anisotropic spectrum will be discussed by comparing it with the computed spectrum in a later section.

3.1.3. Decafluorocyclopentane Radical Anion (c-$C_5F_{10}^-$). Figure 3 shows the temperature-dependent ESR spectra of c-$C_5F_{10}^-$ in the TMS matrix measured in the temperature range

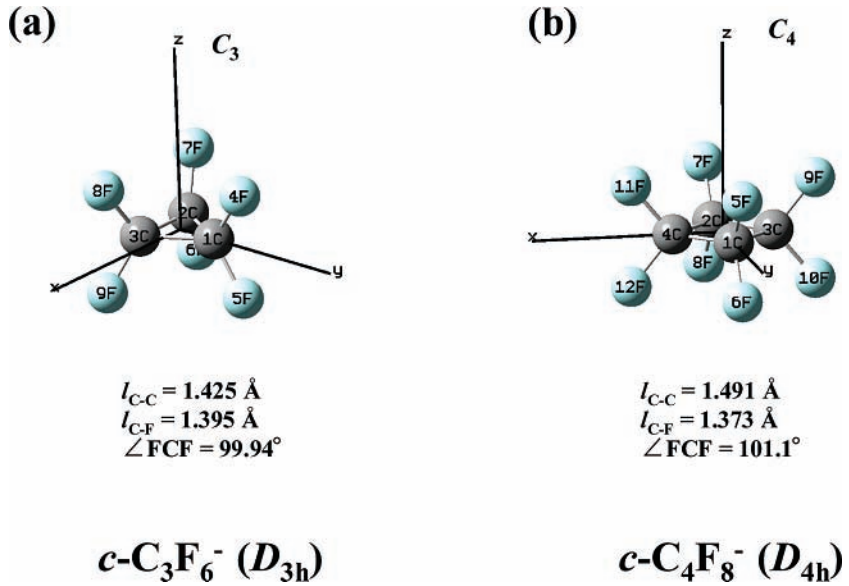

Figure 4. Optimized geometrical structures and point group symmetries (in parentheses) of (a) c-$C_3F_8^-$ and (b) c-$C_4F_8^-$, together with the numbering of the ^{13}C and ^{19}F nucleus positions and the x,y,z coordinate system. The computations were performed using method C.

of 110−162 K. Spectrum (c), recorded at 162 K, is essentially isotropic and can be analyzed in terms of a radical that possesses ten equivalent ^{19}F nuclei, with the line positions corresponding precisely to those expected for the second-order *hf* structure calculated from the averaged isotropic splitting of $a = 11.6$ mT (see Table 1).

Although the ESR spectral lines gradually became broader as the sample temperature was reduced from 162 K to 140 K, the spectrum retained its original isotropic appearance in this temperature range, as shown in spectrum (b), which was recorded at 147 K. After further decreasing the temperature to 110 K, however, the ESR spectrum became anisotropic with a diffuse line shape, especially in the outer regions, as shown in spectrum (a). Because no further appreciable spectral changes were observed after cooling from 110 K to 80 K, the 110 K spectrum can be regarded as being close to the rigid limit. This spectrum can be simulated using the computed principal values and directions of the ^{19}F *hf* splitting tensors, as discussed in a later section.

As shown in Table 1, the averaged isotropic ^{19}F *hf* splittings obtained for c-$C_3F_6^-$, c-$C_4F_8^-$, and c-$C_5F_{10}^-$ in the TMS matrix agree precisely with those previously reported for these radical anions generated and stabilized in the neopentane[15,16] and hexamethylethane[13] (HME) matrices. This excellent agreement suggests that the matrix effects on the ^{19}F *hf* splitting are negligibly small; i.e., the singly occupied molecular orbital (SOMO) and, more specifically, the spin densities of the radical anions are negligibly perturbed by the surrounding matrix molecules. This allows a direct comparison to be made of the experimental ^{19}F *hf* splittings (Table 1) with the theoretical values in Tables 2−4, which have been computed based on the isolated molecule approximation.

After exposure of the c-$C_3F_6^-$ radical anion sample in TMS (Figure 1d) to unfiltered light from a tungsten lamp, all the ESR spectral lines attributable to the radical anion were completely removed, leaving only the intense central band that was due mainly to the $(CH_3)_3SiCH_2$ matrix radical. Identical photobleaching effects were observed for the c-$C_4F_8^-$ and c-$C_5F_{10}^-$ species. These results are not only consistent with the assignment of the lines to a single photolabile species but also support the anionic nature of these radicals, as will be described later in section 3.4, "Electronic Spectra".

3.2. Computational Results: Isotropic and Anisotropic ^{19}F *hf* Splittings and SOMO. A series of quantum chemical computations were conducted independent of the previous studies,[4,12a,13] to further elucidate the geometrical and electronic structures of the c-$C_3F_6^-$, c-$C_4F_8^-$, and c-$C_5F_{10}^-$ radical anions. A particular focus of the present work is on the calculation of the anisotropic ^{19}F *hf* tensors, and their comparison with the experimental results obtained by analyzing the experimental anisotropic ESR spectra. This comparison has previously been limited only to the isotropic ^{19}F *hf* couplings.[13] Hereinafter, we use the following abbreviation: "B3LYP/6-311+G(2df,p)//MP2/6-311+G(d,p)", which will be used to represent ESR hyperfine parameter computations via the B3LYP method (with 6-311+G(2df,p) basis set) for the geometry optimized by the MP2 method (with 6-311+G(d,p) basis set)", etc. The computations were performed using three different methods: (i) method A, B3LYP/6-311+G(2df,p)//B3LYP/6-311+G(d,p); (ii) method B, B3LYP/6-311+G(2df,p)//MP2/6-311+G(d,p); and (iii) method C, B3LYP/6-311+G(2df,p)//UHF/6-311+G(d,p).

3.2.1. c-$C_3F_6^-$. The neutral c-C_3F_6 molecule in D_{3h} geometry has a $^1A_1'$ ground state with a doubly degenerate 7e′ highest occupied molecular orbital (HOMO).[12a,13,28,29] The c-$C_3F_6^+$ radical cation is a Jahn−Teller active species and is expected to be distorted to a C_{2v} structure, in which the originally degenerate HOMO splits into a_1 and b_2 orbitals: the expected ground state is $^2A_1$ (C_{2v}).[28] On the other hand, the lowest unoccupied molecular orbital (LUMO) of c-C_3F_6 consists of a single molecular orbital, and so the c-$C_3F_6^-$ radical anion is not expected to be a first-order Jahn−Teller active species. Consistent with previous reports,[4,12a,13] the electronic ground state of c-$C_3F_6^-$ is $^2A_2''$ in D_{3h} symmetry by all three computational methods. The plots in Figure 5 clearly show that the a_2'' SOMO consists of p_π-type orbitals from the three equivalent C atoms, a nodal plane occurring at the carbon ring, and a set of p_σ-type orbitals from six equivalent ^{19}F atoms. The latter p_σ-type ^{19}F orbitals point toward the center of the carbon ring plane and conform to the C_3 and σ_h symmetry elements. The bond lengths and bond angles computed by the unrestricted Hartree-Fock (UHF) level (method C) are shown in Figure 4a. These results show that the molecular geometry is significantly altered by electron attachment: thus, relative to the values in neutral

c-C_3F_6,[28] the F−C−F angle decreases by ca. 10° and the C−C bond length decreases by ca. 0.1 Å, whereas the C−F bond increases by 0.1 Å. These changes in bond lengths originate from the population in the radical anion of the high-symmetry a_2'' SOMO with its C−C bonding and C−F antibonding characteristics; similar changes in the geometrical parameters are observed to occur upon electron attachment to the other perfluorocycloalkanes with $n = 4$ and 5.

The computed ^{19}F *hf* splittings of c-$C_3F_6^-$ are summarized in Table 2a. Method C closely reproduces the experimental isotropic splitting of $a(^{19}F) = 19.8$ mT for six equivalent ^{19}F nuclei, whereas method A results in a 46% larger $a(^{19}F)$ value and method B gives a 7% smaller $a(^{19}F)$ value. It may also be noted that the experimental geometrical parameters of the neutral molecule[29] are also best reproduced by the UHF computations (method C). The anisotropic ^{19}F *hf* splitting tensors that are computed by all three methods are almost axially symmetric; however, these computed anisotropic splittings cannot be directly compared with the experimental values, as mentioned in section 3.3, "ESR Spectra Involving Anisotropic Couplings: Comparison of Experimental and Computational Results". Figure 5 shows plots of the SOMO projected to the $y-z$, $x-y$, and $z-x$ planes, where the z-axis is the C_3 symmetry axis (see Figure 4a).

3.2.2. c-$C_4F_8^-$. Neutral c-C_4F_8 adopts D_{2d} symmetry in the $^1A_1$ ground state with a C−C−C−C dihedral angle of 17.4° defining the deviation of the puckered ring carbons from planarity.[30] Consistent with previous calculations,[4,12,13] all three computational methods predict that electron attachment to c-C_4F_8 results in a change from D_{2d} to planar D_{4h} symmetry with a $^2A_{2u}$ electronic ground state. This remarkable increase of symmetry on negative ion formation is in sharp contrast to the reduced symmetry that is predicted to occur in the acyclic perfluorocompounds,[12a] and is indicative of a stabilizing effect that results from the more-complete delocalization of the added electron in the planar D_{4h} ring structure. Figure 6 shows plots of the SOMO projected to the $y-z$, $x-y$, and $z-x$ planes, where the z-axis is the C_4 symmetry axis (see Figure 4b).

The SOMO of c-$C_4F_8^-$ is very similar to that of c-$C_3F_6^-$, consisting again of overlapping carbon p_π-type orbitals forming a nodal plane at the planar ring, together with the set of p_σ-type orbitals from the eight equivalent ^{19}F atoms. Because the SOMO is C−C bonding and C−F antibonding, the C−C bond is shortened and the C−F bond is lengthened on electron attachment to c-C_4F_8.[4,12a,13] Also, as indicated in Figure 4b by the calculation at the UHF level (method C), the FCF angle decreases from 110.0° in the neutral molecule (experimental value = 109.9° ± 0.3°)[30] to 101.0° in the negative ion. This brings about an increase of ca. 0.1 Å in the calculated nonbonded F−F distance between neighboring carbons, thereby favoring the reduction in the ring dihedral angle that occurs by changing from the puckered D_{2d} symmetry to the planar D_{4h} symmetry upon electron attachment.[4,12a,13] This adoption of a planar ring geometry leads to findings that parallel those for c-$C_3F_6^-$; the set of p_σ-type orbitals from the ^{19}F atoms in c-$C_4F_8^-$ point approximately toward the ring center and possess the C_4 major axis and σ_h symmetry elements of the D_{4h} point group. The computed *hf* splittings of c-$C_4F_8^-$ are summarized in Table 3a, and all of the methods predict the ^{19}F *hf* tensor to have almost-axial symmetry. The isotropic splitting for eight equivalent ^{19}F nuclei, computed using method C, is again in remarkably good agreement with the experimental value; viz., $a(^{19}F) = 14.85$ mT (exp) vs 14.84 mT (calc). Accordingly, the anisotropic ^{19}F *hf* splittings computed by method C have been used, together

TABLE 2: ESR Parameters Computed for c-$C_3F_6^-$

(a) ^{13}C and ^{19}F Hyperfine Splittings (in mT)

state (symmetry)	exp	$^2A_2''(D_{3h})$	$^2A_2''(D_{3h})$	$^2A_2''(D_{3h})$
ESR (method/basis sets)//geometry		method A:	method B:	method C:
(method/basis sets)		B3LYP/6-311 + G(2df,p)// B3LYP/6-311 + G(d,p)	B3LYP/6-311 + G(2df,p)// MP2/6-311 + G(d,p)	B3LYP/6-311 + G(2df,p)// UHF/6-311 + G(d,p)
^{13}C and ^{19}F isotropic *hf* splittings				
$a(^{13}C)$ (for three ^{13}C)		−0.25	−0.51	−0.56
$a(^{19}F)$ (for six ^{19}F)	19.8 in TMS and Neop	29.32	18.38	19.78
^{19}F anisotropic *hf* splitting				
B_{aa}		−2.71	−5.00	−4.90
B_{bb}		−2.63	−4.91	−4.84
B_{cc}		5.34	9.91	9.75
$<S^2>$ ESR//geometry		0.7509//0.7501	0.7517//0.7606	0.7516//0.7590

(b) Direction Cosines for the Anisotropic ^{13}C and ^{19}F Hyperfine Splittings (in mT)[a]

	Anisotropic *hf* Splittings (Direction Cosines: x,y,z System)[c,d]		
^{13}C and ^{19}F nucleus position[b]	B_{aa}	B_{bb}	B_{cc}
$1^{13}C$	−8.26 (1.0000, 0.0000, 0.0000)	−4.90 (0.0000, 1.0000, 0.0000)	13.16 (0.0000, 0.0000, 1.0000)
$4^{19}F$	−4.90 (0.0000, −0.3007, 0.9537)	−4.84 (1.0000, 0.0000, 0.0000)	9.75 (0.0000, 0.9537, 0.3007)

[a] Computed for the $^2A_2''(D_{3h})$ state using method C. [b] See Figure 4a for the numbering of ^{13}C and ^{19}F nucleus positions and the x,y,z system. [c] The direction cosines for the ^{13}C nuclei at positions 2 and 3 in Figure 4a are obtained by taking into account the C_3 symmetry about the z-axis. [d] The direction cosines for the ^{19}F nuclei at positions 5−9 are obtained by taking into account the D_{3h} symmetry (C_3 symmetry operation about the z-axis and σ_h symmetry).

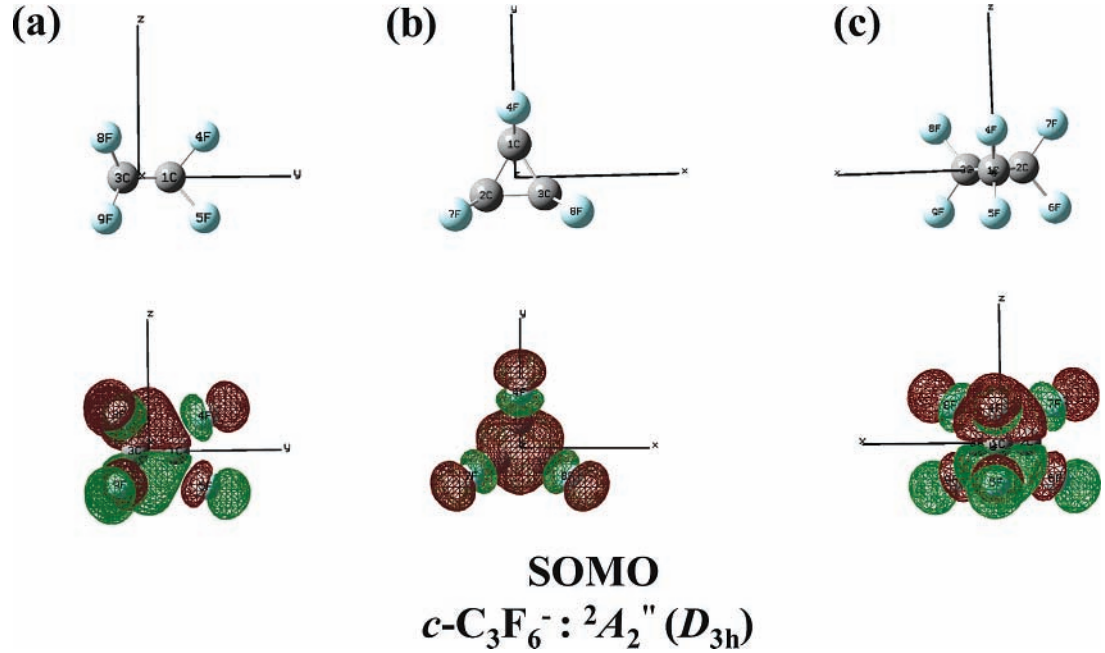

Figure 5. Plots of the singly occupied molecular orbitals (SOMOs) projected to (a) the $y-z$ plane, (b) the $x-y$ plane and (c) the $z-x$ plane computed for c-$C_3F_6^-$ with $^2A_2''$ ground electronic state in D_{3h} point group symmetry. The computations were performed using method C. Refer to Figure 4a for the x,y,z coordinate system.

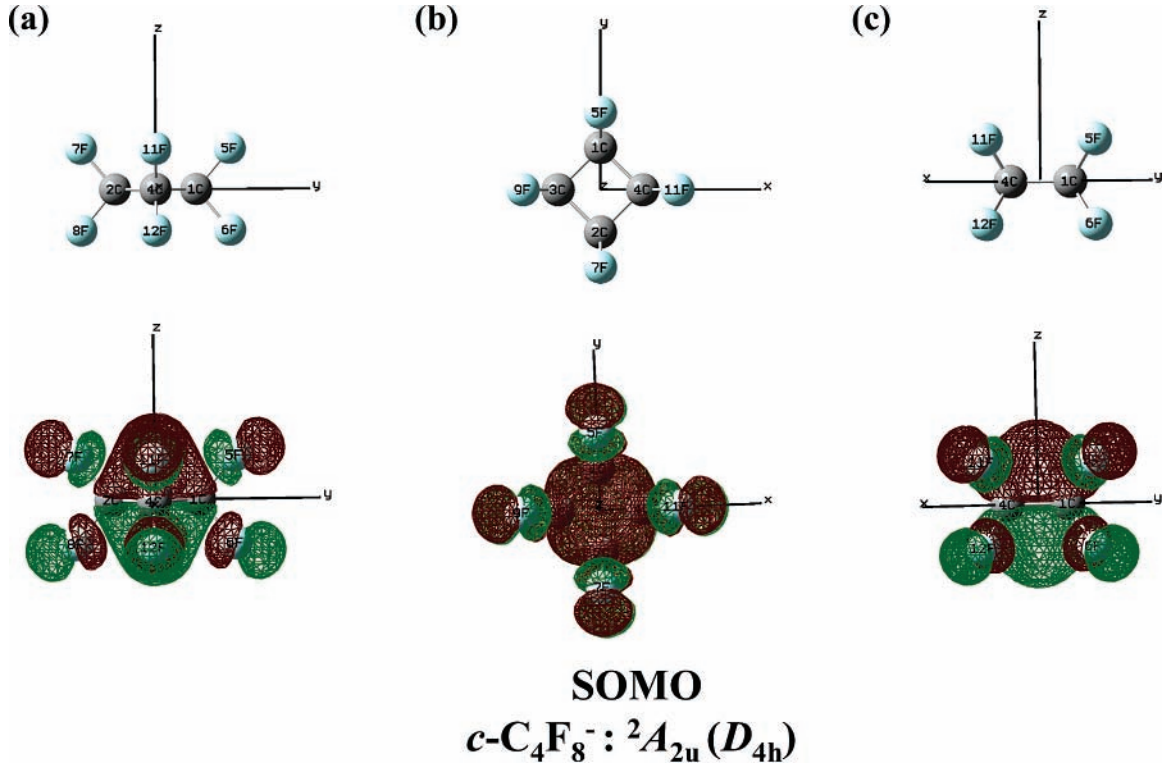

Figure 6. Plots of the SOMOs projected to (a) the $y-z$ plane, (b) the $x-y$ plane, and (c) the plane containing the z-axis and one line, which connects the middle points of the 2C−4C bond and the 1C−3C bond, computed for c-$C_4F_8^-$ with $^2A_{2u}$ ground electronic state in D_{4h} symmetry. The computations were performed using method C. Refer to Figure 4b for the x,y,z coordinate system.

with their direction cosines (Table 3b), to simulate the experimental anisotropic ESR spectrum, as mentioned in section 3.3.

3.2.3. c-$C_5F_{10}^-$. All restricted Hartree−Fock (RHF) computations predict that neutral c-C_5F_{10} adopts a C_s symmetrical structure, although a C_1 structure lies no more than 0.02 kcal/mol above the C_s structure.[13] The computed geometrical structure of c-$C_5F_{10}^-$ is dependent on the method used. Although methods A (B3LYP) and B (MP2) both predict that the c-$C_5F_{10}^-$ negative ion adopts a C_s structure with a $^2A'$ ground state, method C (UHF) predicts a planar D_{5h} symmetry with a $^2A_2''$ ground state, similar to that observed for the c-$C_3F_6^-$ and c-$C_4F_8^-$ negative ions, in agreement with earlier computations using the KMLYP method.[12a]

The ^{19}F hyperfine splittings computed by B3LYP for the c-$C_5F_{10}^-$ ion with C_s and D_{5h} symmetry are summarized in Table 4a. Using method C, the isotropic splitting computed for ten

TABLE 3: ESR Parameters Computed for *c*-$C_4F_8^-$

(a) ^{13}C and ^{19}F Hyperfine Splittings (in mT)

state (symmetry)	exp	$^2A_{2u}$ (D_{4h})	$^2A_{2u}$ (D_{4h})	$^2A_{2u}$ (D_{4h})
ESR (method/basis sets)// geometry (method/basis sets)		method A: B3LYP/6-311+G(2df,p)// B3LYP/6-311+G(d,p)	method B: B3LYP/6-311+G(2df,p)// MP2/6-311+G(d,p)	method C: B3LYP/6-311+G(2df,p)// UHF/6-311+G(d,p)
^{13}C and ^{19}F isotropic *hf* splittings				
$a(^{13}C)$ (for four ^{13}C)		−0.55	−0.54	−0.53
$a(^{19}F)$ (for eight ^{19}F)	14.85 in TMS	13.17	13.66	14.84
^{19}F anisotropic *hf* splitting				
B_{aa}		−3.73	−3.67	−3.54
B_{bb}		−3.63	−3.59	−3.48
B_{cc}		7.36	7.26	7.02
$<S^2>$ ESR//geometry		0.7512//0.7511	0.7512//0.7564	0.7511//0.7555

(b) Direction Cosines for the Anisotropic ^{13}C and ^{19}F Hyperfine Splittings (in mT)[a]

^{13}C and ^{19}F nucleus position[b]	Anisotropic *hf* Splittings (Direction Cosines: *x*,*y*,*z* System)[c,d] B_{aa}	B_{bb}	B_{cc}
$1^{13}C$	−0.52 (1.0000, 0.0000, 0.0000)	−0.29 (0.0000, 1.0000, 0.0001)	0.81 (0.0000, −0.0001, 1.0000)
$5^{19}F$	−3.54 (0.0000, −0.2659, 0.9640)	−3.48 (1.0000, 0.0000, 0.0000)	7.02 (0.0000, 0.9640, 0.2659)

[a] Computed for the $^2A_{2u}$ (D_{4h}) state using method C. [b] See Figure 4b for the numbering of ^{13}C and ^{19}F nucleus positions and the *x*,*y*,*z* system. [c] The direction cosines for ^{13}C nucleus positions 2, 3, and 4 are obtained by sign change of the *x*- and *y*-components of $1^{13}C$ by a C_4 symmetry operation about the *z*-axis. [d] The direction cosines for the other ^{19}F nucleus positions (6−12) are obtained by change of the *x*-, *y*-, and *z*-components of $5^{19}F$ by taking a D_{4h} symmetry into consideration (a C_4 symmetry operation about the *z*-axis and σ_h symmetry operations).

equivalent ^{19}F nuclei in the D_{5h} structure is again in surprisingly good agreement with the experimental value. However, as shown in Table 4a, a similarly good agreement with experiment is obtained by method B for the average value of the computed isotropic splittings for the C_s structure, which consists of six different types of ^{19}F nuclei. In the section on anisotropic ESR spectra, an essentially "static" D_{5h} structure will be considered in terms of a very rapid dynamical averaging of the five possible C_s structures. Figure 8 shows plots of the SOMO computed for the D_{5h} structure by method C; the SOMO being projected to the *y*-*z*, *x*-*y*, and *z*-*x* planes, where the *x*-axis is a C_5 symmetry axis (Figures 7 and 8).

The computed C_s and D_{5h} structures of *c*-$C_5F_{10}^-$ also have the C−C bond compressed and the C−F bond elongated, relative to the neutral molecule. These changes in the bond lengths can originate from the high-symmetry SOMO with the C−C bonding and C−F antibonding characters; similar changes in the geometrical parameters were observed in the other perfluorocycloalkane radical anions with $n = 3$ and 4 studied in this paper.

3.3. ESR Spectra Involving Anisotropic Couplings: Comparison of Experimental and Computational Results.

3.3.1. c-$C_3F_6^-$. Figure 9a shows the anisotropic ESR spectrum of *c*-$C_3F_6^-$ in TMS recorded at 82 K. The spectral pattern is quite complicated, with a large number of line components, many of them being quite sharp in appearance and others having a characteristic anisotropic line shape. Clearly, this "powder" pattern cannot be simply analyzed based on six anisotropically equivalent ^{19}F nuclei, as would be the case if each of the fluorines possessed axially symmetric tensors about a common molecular axis. Moreover, it is very difficult to analyze the experimental spectrum and evaluate the ^{19}F *hf* tensors based on the use of the ordinary trial method for ESR spectral simulation, because of the large number of adjustable parameters that are needed; thus, in addition to the principal values (three parameters) of the ^{19}F *hf* tensor, their directions (three parameters) must also be specified for each of the six ^{19}F nuclei, and the latter are most unlikely to be equivalent in the rigid limit.[14]

Fortunately, recent advances in the B3LYP and MP2 computational methods provide an independent theoretical approach to this difficult spectral simulation problem. As mentioned previously, the experimental isotropic ^{19}F *hf* splittings for *c*-$C_3F_6^-$ are reproduced with very high accuracy by the DFT [B3LYP/6-311+G(2df,p)] computations for the D_{3h} geometry optimized by the UHF/6-311+G(d,p) method (method C in Table 2); *viz.*, $a = 19.8$ mT (exp) vs 19.78 mT (calc) for the six equivalent ^{19}F nuclei. This excellent agreement in the isotropic ^{19}F *hf* splittings encouraged us to simulate an anisotropic "powder" spectrum that involved anisotropic couplings of *c*-$C_3F_6^-$, using the computed hyperfine principal values and directions of ^{19}F nuclei,[14] and the theoretical ESR spectrum simulated using the ^{19}F *hf* tensors in Table 2b is compared with the experimental spectrum in Figure 9b. The overall spectral features are reproduced quite well by the computations, especially in regard to both the detailed fine structure and the outermost anisotropic features, indicated by the vertical bars in Figure 9. The total spectral width measured between these outermost features is 133.4 mT, which is only 0.7 mT larger than the experimental result (132.7 mT); therefore, the error, with respect to the observed total splitting, is only 0.5%. Thus, we conclude that the computed anisotropic ^{19}F *hf* coupling tensors (the principal values of the *hf* splittings and their

TABLE 4: ESR Parameters Computed for *c*-$C_5F_{10}^-$

(a) ^{13}C and ^{19}F *hf* Splittings (in mT)

state (symmetry)	exp	^2A (C_s)	^2A (C_s)	$^2A_2''$ (D_{5h})
ESR (method/basis sets)// geometry (method/basis sets)		method A: B3LYP/6-311+G(2df,p)// B3LYP/6-311+G(d,p)	method B: B3LYP/6-311+G(2df,p)// MP2/6-311+G(d,p)	method C: B3LYP/6-311+G(2df,p)// UHF/6-311+G(d,p)
^{13}C isotropic *hf* splittings, $a(^{13}C)$[a] (for five ^{13}C)				
average[a]		0.51	0.50	0.50 ± 0.1
$1^{13}C$ and $2^{13}C$		0.51	0.50	
$3^{13}C$ and $4^{13}C$		0.52	0.51	
$5^{13}C$		0.50	0.49	
^{19}F isotropic *hf* splittings, $a(^{19}F)$[b] (for ten ^{19}F)				
average[b]	11.6 in TMS	10.70	11.51	11.65 ± 0.01
$14^{19}F$		14.04	16.72	
$7^{19}F$ and $8^{19}F$		13.46	15.86	
$10^{19}F$ and $13^{19}F$		11.80	13.30	
$11^{19}F$ and $12^{19}F$		9.66	9.82	
$6^{19}F$ and $9^{19}F$		7.96	7.10	
$15^{19}F$		7.35	6.19	
^{19}F anisotropic *hf* splitting, (B_{aa}, B_{bb}, B_{cc})				
$6^{19}F$ and $9^{19}F$			(−2.02, −1.97, 3.99)	For ten ^{19}F nuclei: (−2.62, −2.56, 5.18)
$7^{19}F$ and $8^{19}F$			(−3.67, −3.53, 7.19)	
$10^{19}F$ and $13^{19}F$			(−3.28, −3.18, 6.46)	
$11^{19}F$ and $12^{19}F$			(−2.61, −2.53, 5.14)	
$14^{19}F$			(−3.74, −3.59, 7.33)	
$15^{19}F$			(−1.81, −1.77, 3.58)	
$<S^2>$ ESR//geometry		0.7509//0.7508	0.7509//0.7550	0.7508//0.7536

(b) Direction Cosines for the Anisotropic ^{13}C and ^{19}F *hf* Splittings (in mT) for $^2A_2''$ (D_{5h}) State[c]

^{13}C and ^{19}F nucleus position[d]	Anisotropic *hf* Splittings (Direction Cosines: *x*,*y*,*z* System)[e] B_{aa}	B_{bb}	B_{cc}
$1^{13}C$	−0.35 (0.0000, 0.9510, 0.3092)	−0.21 (0.0001, −0.3092, 0.9510)	0.56 (1.0000, 0.0000, 0.0001)
$14^{19}F$	−2.62 (0.9717, −0.2361, 0.0000)	−2.56 (0.0000, 0.0000, 1.0000)	5.18 (0.2361, 0.9717, 0.0000)

[a] Averaged value over five ^{13}C *hf* splittings. [b] Averaged value over ten ^{19}F *hf* splittings. [c] Computed for the $^2A_2''$ (D_{5h}) state using method C. [d] See Figure 7a for the numbering of ^{13}C and ^{19}F nucleus positions and the *x*,*y*,*z* system. [e] The direction cosines for ^{13}C nucleus positions 2, 3, 4, and 5 and those for the ^{19}F and nucleus positions 6−13 and 15 are obtained by sign change of the *x*-, *y*-, *z*-components of $1^{13}C$ and $14^{19}F$ by taking the D_{5h} symmetry into consideration (a C_5 symmetry operation about the *y*-axis and σ_h symmetry operation).

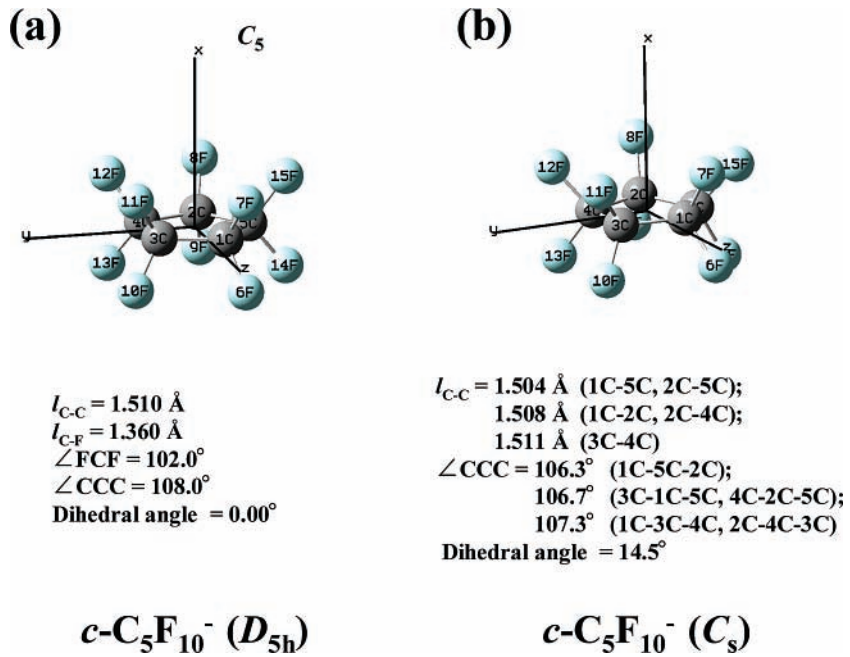

Figure 7. Geometrical structures optimized for the *c*-$C_5F_{10}^-$ radical anion with (a) D_{5h} structure with $^2A_2''$ ground electronic state and (b) C_s structure with $^2A'$ state, together with the numbering of the ^{13}C and ^{19}F nucleus positions and the *x*,*y*,*z* coordinate system. The computations were performed using methods C and B, respectively.

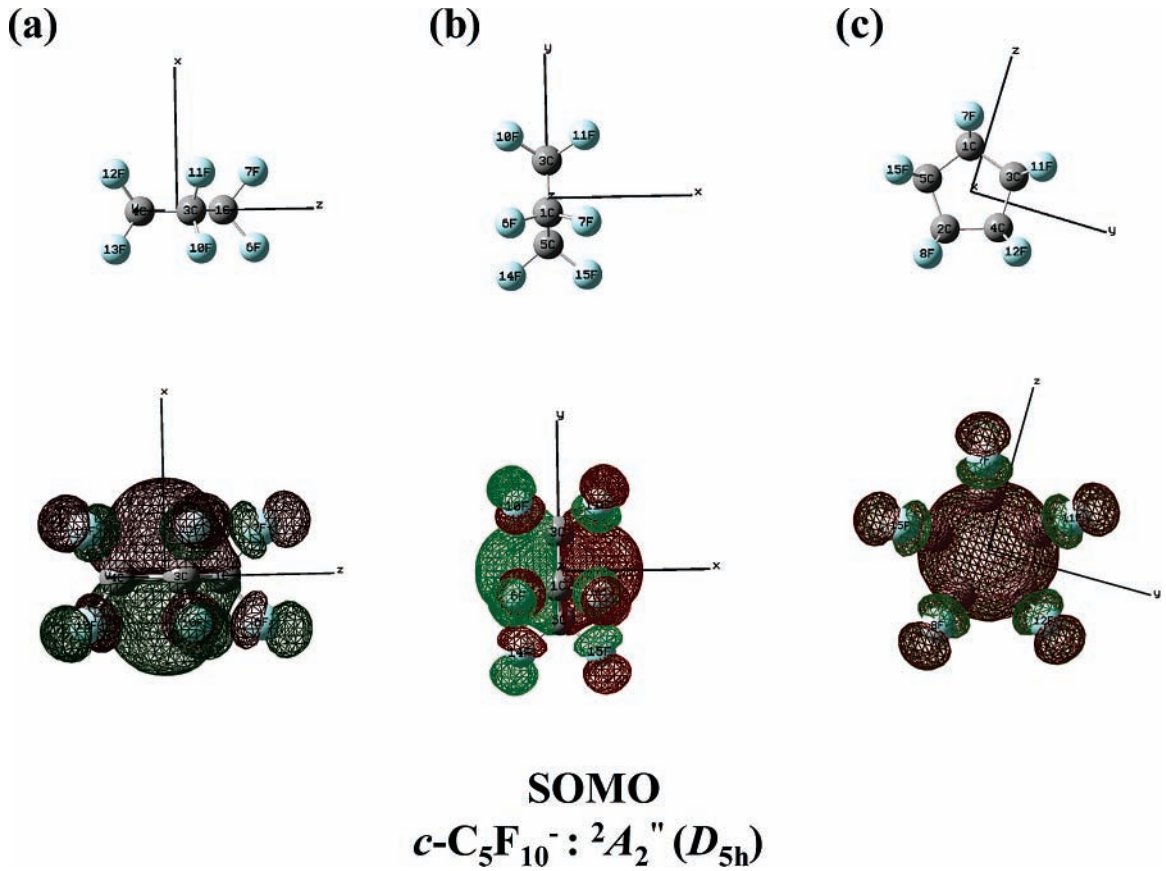

Figure 8. Plots of the SOMOs projected to (a) the $z-x$ plane, (b) the $x-y$ plane, and (c) the $y-z$ plane computed for *c*-$C_5F_{10}^-$ with $^2A_2''$ electronic state in D_{5h} point group symmetry. The computations were performed using method C. Refer to Figure 7a for the *x*,*y*,*z* coordinate system.

directions) are quite close to the experimental values, paralleling the excellent agreement observed for the isotropic ^{19}F *hf* splittings.

The present computations all assign the *c*-$C_3F_6^-$ radical anion to the $^2A_2''$ electronic ground state (in D_{3h} symmetry) with six magnetically equivalent ^{19}F nuclei, with the predicted ^{19}F *hf* splitting being in excellent agreement (Table 1) with the previous results of isotropic ESR studies.[13,15,16] Turning to the anisotropic ^{19}F *hf* splittings, those computed by method C display almost-perfect axial symmetry: (B_{aa}, B_{bb}, B_{cc}) = (−4.90 mT, −4.84 mT, +9.75 mT). Using the direction cosines in Table 2, it is determined that the principal directions of B_{cc}, corresponding

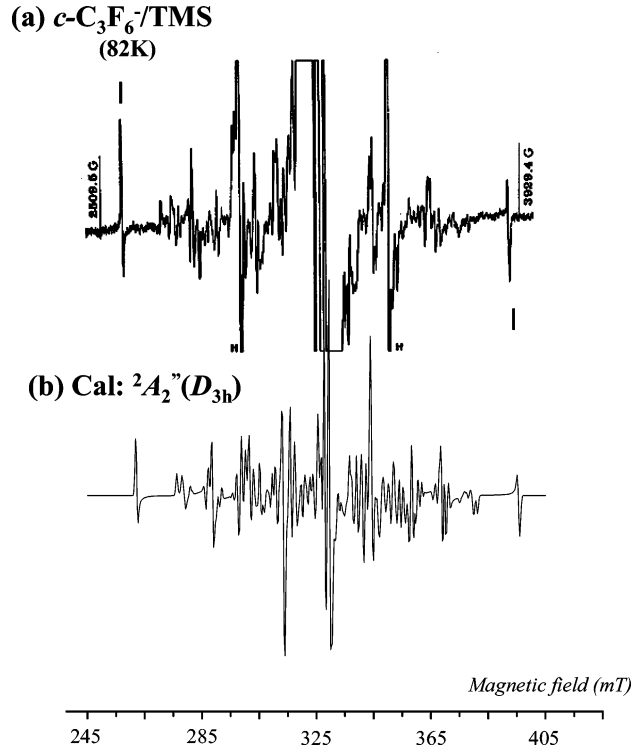

Figure 9. (a) ESR spectrum of c-$C_3F_6^-$ in TMS at 82 K ($\nu = 9117.5$ Hz), and (b) theoretical ESR spectrum of c-$C_3F_6^-$ computed using the principal values and principal directions of ^{19}F ($I = {}^1/_2$) *hf* splittings via method C given in Table 2. In the spectral computations, a constant Gaussian line width of 0.7 mT was used. The vertical bars correspond to the outermost anisotropic doublet (M_I, $I = \pm 3, 3$). See text for more detail. (10 G = 1 mT.)

to the maximum ^{19}F anisotropic splittings, lie in the $y-z$ plane with an angle of $\pm 17.5°$, measured from the y-axis, as shown in Figure 10, for the (4F and 5F) pair of nuclei. Furthermore, the principal directions of B_{cc} should occur along the directions suggested by the axes that define the cylindrical cross section of the spin density (SD) plots. This correspondence is verified for c-$C_3F_6^-$ in Figure 10, where the axes of the SD plots for the (4F and 5F) pair lie in the $y-z$ plane with the same angle ($\pm 17.5°$), measured from the y-axis, as B_{cc}, with the principal directions of the SD plots therefore being parallel to B_{cc}. Moreover, it is observed that the SD plots are very similar to those of the SOMO, as shown in Figures 5a and 10. Such close agreement between the SD and the SOMO can be observed not only for c-$C_3F_6^-$, but also for the other perfluorocycloalkane radical anions studied here, as will be mentioned later. The principal directions of B_{cc} for the other two pairs of ^{19}F-nuclei in c-$C_3F_6^-$, denoted by (6F and 7F) and (8F and 9F), can be obtained from those of the (4F and 5F) pair by a C_3 symmetry operation about the z-axis; these are again parallel to the corresponding SOMO and SD axes.

3.3.2. c-$C_4F_8^-$. Figure 11a shows the anisotropic ESR spectrum of c-$C_4F_8^-$ generated by γ-irradiation in a rigid MTHF matrix and recorded at 77 K. Although the central portion of the c-$C_4F_8^-$ spectrum is obscured by a strong quintet pattern from the matrix radical, the anisotropic *hf* features present in both wings are attributable to the rigid-state spectrum of c-$C_4F_8^-$.

Consistent with other studies,[4,12,13] all the present computations (Table 3a) assign the c-$C_4F_8^-$ radical anion to the $^2A_{2u}$ ground electronic state (in D_{4h} symmetry). The calculated isotropic ^{19}F splitting of c-$C_4F_8^-$, using method C, is, again, in almost-perfect agreement (Table 3a) with the experiment: viz., $a = 14.85$ mT (exp) vs 14.84 mT (calc) for the eight equivalent ^{19}F nuclei. Accordingly, the isotropic and anisotropic ^{19}F *hf* splittings, together with their direction cosines computed by method C (Table 3b), were then chosen to simulate the rigid-limit ESR spectrum of c-$C_4F_8^-$. As shown in Figure 11, the overall spectral features are simulated quite well, especially in the regions lying outside the two hydrogen-atom lines (marked as "H"). Furthermore, the error in the total splitting is as small as 0.4% of the experimental spectral width; viz., 137.0 mT (exp) vs 136.5 mT (calc). Thus, we confirm that, as with c-$C_3F_6^-$, the ^{19}F *hf* tensors computed for c-$C_4F_8^-$ via the present computations, using method C, are very similar to the actual values.

The anisotropic ^{19}F *hf* splittings computed by method C (Table 3b) and used for the spectral calculations are (B_{aa}, B_{bb}, B_{cc}) = (−3.54 mT, −3.48 mT, +7.02 mT); these are again almost axially symmetric. It is also observed, from the direction cosines of the anisotropic splittings in the table, that the principal directions of B_{cc} for the 5F, 6F, 7F, and 8F nuclei lie in the $y-z$ plane with an angle of $\pm 15.4°$ from the y-axis, as shown in Figure 12; this angle is ca. 2° smaller than that in c-$C_3F_6^-$. Furthermore, it is easy to see from the figure that the principal directions of B_{cc} for the other four ^{19}F nuclei (9F−12F) lie in the $z-x$ plane with the same angle of $\pm 15.4°$, measured from the x-axis, i.e., these directions possess C_4 symmetry about the molecular z-axis. It, again, can be observed that the principal directions of B_{cc} occur along the directions suggested by the plots of SD and SOMO, as shown in Figure 6a and 12.

3.3.3. c-$C_5F_{10}^-$. Figure 13a shows an anisotropic spectrum of c-$C_5F_{10}^-$ in TMS recorded at 110 K. As mentioned in section 3.2, the computations via method C resulted in a D_{5h} structure, with the C atoms being coplanar and ten magnetically equivalent ^{19}F atoms. The isotropic ^{19}F *hf* splitting computed for the D_{5h} structure reproduces the experimental value quite well; viz., $a = 11.7 \pm 0.1$ (exp) vs 11.65 (cal) (Tables 1 and 4a). On the other hand, computations made via method B resulted in a C_s structure with the C atoms not being coplanar and six different types of ^{19}F nuclei. The average value of the isotropic ^{19}F *hf* splittings computed for the C_s structure is $a = 11.51$ mT, which also closely reproduces the experimental value.

Theoretical ESR spectra were simulated for c-$C_5F_{10}^-$, using the ^{19}F *hf* tensors computed for both the planar D_{5h} and nonplanar C_s structures and are shown in Figures 13b and 13c. These two calculated spectra show marked differences, and only the spectrum calculated for the D_{5h} structure reproduces the seven broad anisotropic features in the experimental spectrum. In contrast, the spectrum calculated for the C_s structure consists of many additional anisotropic *hf* lines resulting from the many different *hf* splittings, and is in much poorer agreement with the experimental spectrum. Thus, although such nonplanar C_s structures are predicted by the B3LYP (method A) and MP2 (method B) methods as in the previous studies,[12a,13] we tentatively conclude, based on this consideration of anisotropic ESR spectra, that the c-$C_5F_{10}^-$ radical anion effectively adopts a planar D_{5h} structure in the rigid limit with a $^2A_2''$ electronic ground state. This effective structure could result from a dynamical averaging over the five equivalent C_s conformations or from a highly symmetric frozen D_{5h} geometry. The experimental data are not sufficiently resolved to distinguish between the two cases.

In fact, the better fit of the anisotropic spectrum of c-$C_5F_{10}^-$ at 110 K to the simulation based on the D_{5h} structure rather than the C_s structure is consistent with theoretical calculations, showing that there is only a very small energy difference between the D_{5h} second-order saddle point and the C_s minimum.

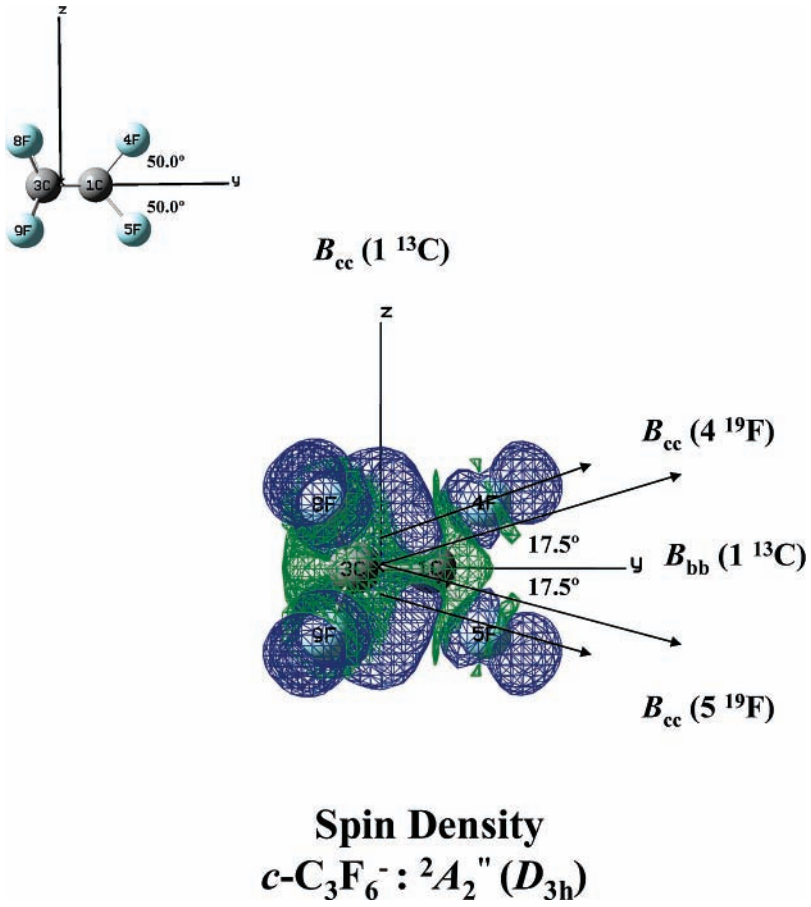

Figure 10. Plots of the spin density (SD) projected to the $y-z$ plane computed for c-$C_3F_6^-$ with the $^2A_2''$ (D_{3h}) electronic state. The computations were performed using method C. The principal directions of ^{13}C *hf* splitting at position 1 (1^{13}C) and ^{19}F *hf* splittings at positions 4 and 5 (4^{19}F and 5^{19}F) are indicated in the figure. Refer to Figures 4a and 5a for the *x,y,z* coordinate system and Table 2b for the *hf* principal directions and values.

This "planarization energy" is given as 0.15 kcal/mol in the paper by Schaefer and co-workers[12a] and "less than 0.2 kcal/mol" by El-Sohly et al.[13] Taking the former estimate of 0.15 kcal/mol as the free-energy barrier between equivalent C_s structures, the Eyring equation[31] suggests that the rate constant for such ring inversion at 100 K would be close to 10^{12} s^{-1} or 10^6 MHz. This frequency greatly exceeds the computed ^{19}F *hf differences* (ca. 100 MHz) for the C_s structure given by methods A and B in Table 4a. Therefore, according to this analysis, a fluxional or averaged D_{5h} structure is likely to persist at ca. 100 K and the C_s rigid-limit structure would only contribute to the anisotropic spectrum at <10 K.

The anisotropic ^{19}F *hf* splittings computed for the D_{5h} structure by method C and used for the spectral simulations are (B_{aa}, B_{bb}, B_{cc}) = (−2.62 mT, −2.56 mT, +5.18 mT), as listed in Table 4b. Just as with c-$C_3F_6^-$ and c-$C_4F_8^-$, these anisotropic splittings have almost axial symmetry. The principal directions of B_{cc} at the 14F and 15F nuclei lie in the $x-y$ plane with an angle of ±13.5° (again, ca. 2° smaller than that for c-$C_4F_8^-$) from the *y*-axis, as shown in Figure 14. The principal directions of B_{cc} at the other eight ^{19}F nuclei deviate by the same angle of ±13.5° from the molecular $y-z$ plane and are obtained by a C_5 symmetry operation about the molecular *x*-axis, as can easily be seen from Figures 8 (plots of SOMO) and 14 (plots of spin density).

3.3.4. Effective ^{19}F Hyperfine Couplings. We now consider, in more detail, the prominent anisotropic spectral features in both the experimental and computed anisotropic ESR spectra of c-$C_4F_8^-$ (in D_{4h} structure). Because of the highly symmetric nature of the a_{2u} SOMO, the same ^{19}F *hf* splitting is expected for all eight ^{19}F nuclei of c-$C_4F_8^-$ along the *z*-axis (C_4 symmetry axis). Using the standard formulas,[32] the ^{19}F *hf* splitting along the *z*-axis is evaluated to be 12.35 mT from the isotropic (a = 14.84 mT) and anisotropic *hf* splittings (B_{aa}, B_{bb}, B_{cc}) computed by method C and listed in Table 3b.

In the $x-y$ plane, which makes an angle of only 15.4° with the individual B_{cc} directions that correspond to the maximum ^{19}F *hf* tensor splitting, two different ^{19}F *hf* splittings that originate from the two diagonally placed sets of four equivalent nuclei ([5F, 6F, 7F, 8F] and [9F, 10F, 11F, 12F]) are expected (see Figures 4b, 6, and 12). The ^{19}F splitting for each set is quite anisotropic, with a variation of ca. 10 mT; thus, when the applied external magnetic field is varied from the *x*-axis to the *y*-axis, the splitting changes from 11.36 mT to 21.29 mT for one set and vice versa for the other set, as can be seen in Figure 15. However, by considering the effective splitting averaged over the two sets of fluorines in the $x-y$ plane to be one-half the sum of the two ^{19}F *hf* splittings, the angular-dependent splitting changes only from 16.32 mT to 17.06 mT, such that the variation is reduced to 0.74 mT. These minimum and maximum splittings appear at angles of 0° (or 90°) and 45° from either the *x*- or *y*-axis, respectively, with the two sets of four fluorines being nonequivalent at 0° (or 90°) but equivalent at 45°.

It is suggested that the effective splitting along these two directions of high symmetry in the $x-y$ plane can readily account for the two pairs of outermost features that appear in both the simulated and experimental anisotropic spectra in Figure 11. Accordingly, the total spectral widths for the two pairs of outermost features are predicted to be $8 \times 17.06 = 136.5$ mT and 8×16.32 (or $4 \times 11.36 + 4 \times 21.29$) = 130.6

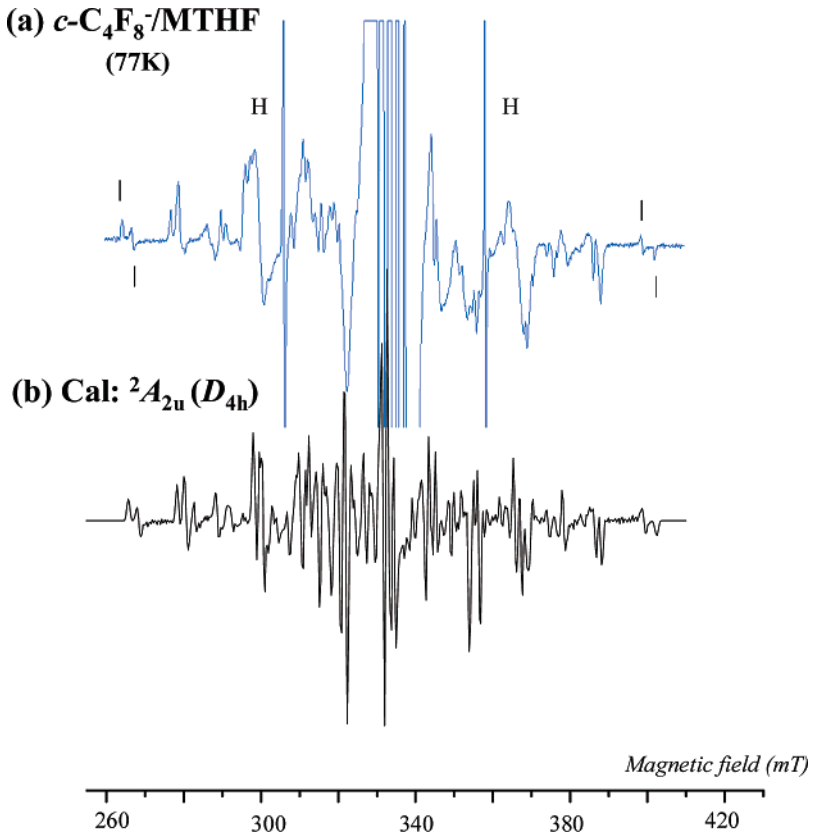

Figure 11. (a) ESR spectrum of c-$C_4F_8^-$ for a 77 K γ-irradiated solid solution of 1 mol % c-C_4F_8 in 2-methyltetrahydrofuran (MTHF) recorded at the same temperature. (b) Theoretical ESR spectrum of c-$C_4F_8^-$ computed using the principal values and principal directions of ^{19}F ($I = {}^1/_2$) hf splittings via method C given in Table 3. In the spectral computations, a constant Gaussian line width of 0.7 mT was used. The vertical bars correspond to the two pairs of outermost anisotropic lines. See text for more detail.

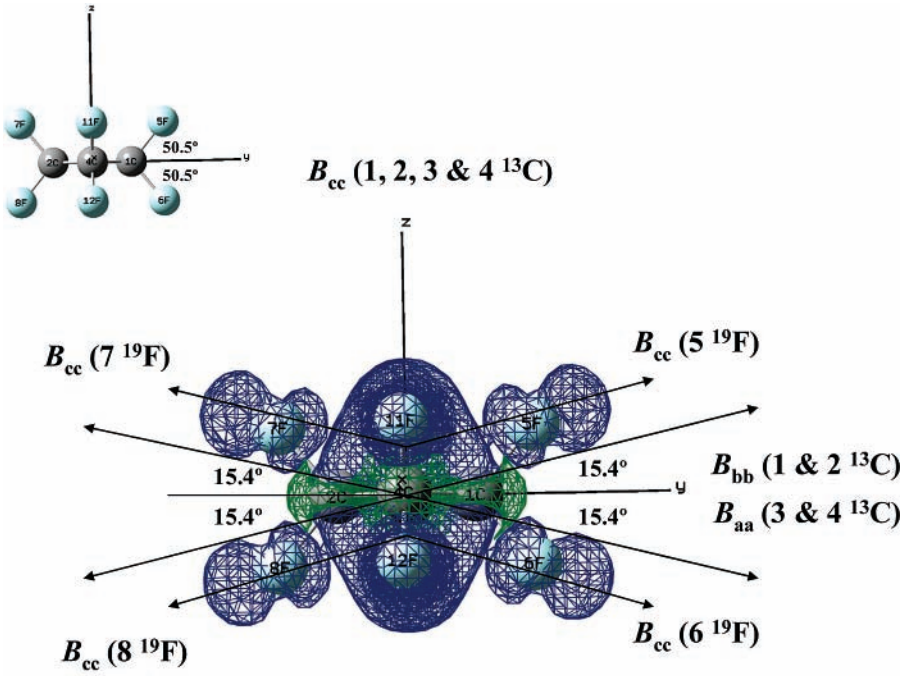

Spin Density
c-$C_4F_8^-$: $^2A_{2u}$ (D_{4h})

Figure 12. Plots of the SD projected to the $y-z$ plane computed for c-$C_4F_8^-$ with the $^2A_{2u}$ (D_{4h}) electronic state. The computations were performed using method C. The principal directions of ^{13}C hf splittings at positions 1, 2, 3, and 4 ($1^{13}C$, $2^{13}C$, $3^{13}C$, and $4^{13}C$) and ^{19}F hf splittings at positions 5, 6, 7, and 8 ($5^{19}F$, $6^{19}F$, $7^{19}F$, and $8^{19}F$) are indicated in the figure. Refer to Figures 4b and 6a for the x,y,z coordinate system and Table 3b for the hf principal directions and values.

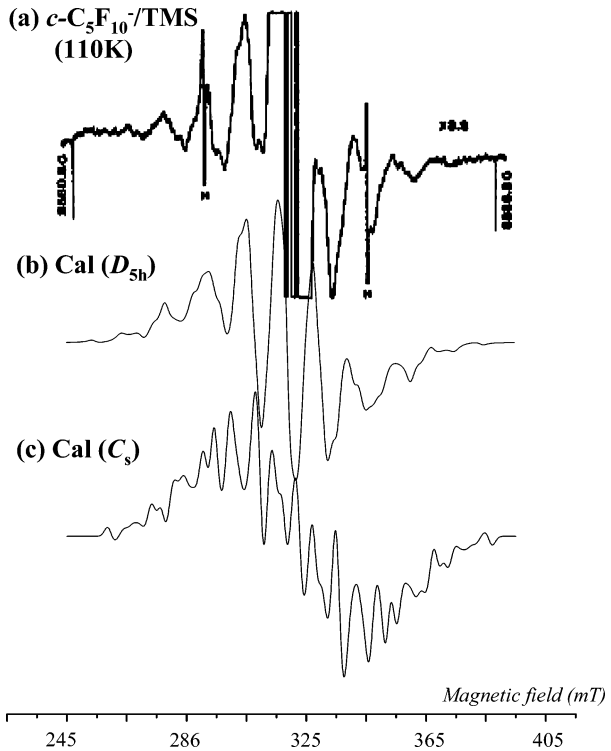

Figure 13. (a) ESR spectrum of c-$C_5F_{10}^-$ in TMS at 110 K ($\nu = 9117.5$ Hz), and theoretical ESR spectrum of c-$C_5F_{10}^-$ computed for (b) $^2A_2''$ (D_{5h}) state and (c) $^2A'$ (C_s) state. The principal values and principal directions of ^{19}F ($I = 1/_2$) *hf* splittings used were computed via method C and via method B, given in Table 4 and Tables 3 and 4 in the Supporting Information. In the spectral computations, a constant Gaussian line width of 2.4 mT was used. (10 G = 1 mT.)

mT. These values, which have been derived based on the computed ^{19}F *hf* tensor splittings, are in good agreement with the experimental widths of 137.0 and 130.9 mT, with this experimentally observed anisotropy of ca. 6.1 mT agreeing nicely with the calculated value of 5.9 mT. Although the lineshapes of these two pairs of outermost features are somewhat reminiscent of parallel and perpendicular components in axial symmetry, the present analysis reveals a much-reduced non-axial *hf* anisotropy (0.74 mT), as compared to that ($21.29 - 11.36 = 9.93$ mT) of the individual and an almost axially symmetric ^{19}F *hf* tensor.

To estimate the isotropic ^{19}F splitting from the aforementioned analysis of the anisotropic ESR spectral features, the splitting along the *z*-axis must also be taken into account. The latter is not separately observable in the experimental spectrum, because the resonance lines are inside the spectrum and overlapped with other lines. However, the previously computed value of 12.35 mT, together with the effective splittings in the $x-y$ plane (17.06 and 16.32 mT) leads to an isotropic splitting of 15.24 mT, which is in satisfactory agreement with the experimental isotropic splitting of 14.9 mT. In summary, the computed spectral widths for the outermost pair of anisotropic ^{19}F *hf* features are consistent with the experimental values, and the derived isotropic ^{19}F splitting is within 2% of the independently determined experimental value.

It is of interest to compare the aforementioned results for c-$C_4F_8^-$ with those for c-$C_3F_6^-$. The same splitting is expected along the *z*-axis for all six ^{19}F nuclei of c-$C_3F_6^-$ (see Figures 5 and 10) and is calculated to be 16.74 mT from the isotropic ($a = 19.78$ mT) and anisotropic *hf* splittings (B_{aa}, B_{bb}, B_{cc}) in Table 2b,[32] together with the 72.5° angle made by B_{cc} with the *z*-axis (Figure 10). In the $x-y$ plane, however, consideration of Figure 5 suggests that different *hf* splittings are expected from three groups of two ^{19}F nuclei ([4F, 5F], [6F, 7F], and [8F, 9F]). Although the individual splittings are quite anisotropic, the average of the three ^{19}F *hf* splittings, one from each group, in the $x-y$ plane varies by only 0.16 mT, from 22.15 mT to 22.31 mT, with a mean of 22.23 mT. Hence, the anisotropy in the $x-y$ plane is expected to be considerably smaller than that for c-$C_4F_8^-$. In fact, the sharp outermost features observed in the experimental and computed spectra (Figure 9) are well-separated from the remainder of the line spectrum, in contrast to the finding of the quite well-resolved and closely spaced twin outermost features observed for c-$C_4F_8^-$. Also, the asymmetric line shape of the c-$C_3F_6^-$ outermost features is consistent with the rather small angular variation of the effective splittings in the $x-y$ plane (0.16 mT), which leads to a difference of spectral widths ($6 \times 0.16 = 0.96$ mT) that is comparable to or only slightly greater than the intrinsic line width in the solid state (0.5−1.0 mT). Thus, the remarkably sharp and singular outermost features in the anisotropic spectrum of c-$C_3F_6^-$ are nicely accounted for by this analysis. A similar small apparent anisotropy is also predicted for the D_{5h} c-$C_5F_{10}^-$ anion; however, in this case, the experimental spectrum is not sufficiently resolved to make a detailed analysis.

There is also good quantitative agreement between the results of theoretical calculations and the experimental values for the ^{19}F *hf* spectral parameters of c-$C_3F_6^-$. First, the effective anisotropic splittings of 22.31 and 22.15 mT in the $x-y$ plane and 16.74 mT in the *z*-direction lead to a calculated isotropic splitting of 20.4 mT, as compared to the experimental value of 19.8 mT. Second, the expected spectral extent for the outermost features of $6 \times 22.23 = 133.4$ mT obtained from the mean 22.23 mT splitting in the $x-y$ plane is within 1% of the 132.7 mT spectral width measured directly from the experimental spectrum in Figure 9.

3.4. Electronic Spectra. Electronic excitation energies and oscillator strengths were computed for the ground electronic states of these perfluorocycloalkane radical anions: viz., c-$C_3F_6^-$ with a $^2A_2''$ (D_{3h}) state, c-$C_4F_8^-$ with a $^2A_{2u}$ (D_{4h}) state, and c-$C_5F_{10}^-$ with a $^2A_2''$ (D_{5h}) state. In Figure 16, their oscillator strengths (f) are plotted in the 200−700 nm range. (For the numerical values, refer to Table 5 in the Supporting Information.) Weak absorptions with $f \approx 0.02-0.03$ are predicted in the visible range of 400−700 nm with $\lambda_{max} = 561$, 535, and 535 nm for c-$C_3F_6^-$, c-$C_4F_8^-$, and c-$C_5F_{10}^-$, respectively. For all three radical anions, the visible-range absorptions that correspond to the lowest excitation energies can be attributed to the electronic transitions from the SOMO to the LUMO: $5a_2'' \Longrightarrow 7a_1'$ for c-$C_3F_6^-$, $5a_{2u} \Rightarrow 6a_{1g}$ for c-$C_4F_8^-$, and $6a_2'' \Rightarrow 8a_1'$ for c-$C_5F_{10}^-$. Furthermore, Figure 16 shows that an increase in the molecular size of c-$C_nF_{2n}^-$ from $n = 3$ to $n = 4$ and 5 results in a "blue" shift with slightly increasing oscillator strengths.

The prediction of light absorption in the visible region is of special interest, in regard to the present experimental results, showing that all the ESR spectral lines attributable to the radical anions are removed by exposure of the sample to unfiltered light from a tungsten lamp. Experimental electronic spectra of the perfluorocycloalkane radical anions are not available in the literature, so the present computations provide new information about the excitation energies and oscillator strengths of these fundamentally important chemical species. The reactivity of these c-$C_nF_{2n}^-$ excited states is also of interest, considering the photobleaching effect by visible light. Potentially, these excited states may undergo either electron detachment, in which case the released electron can combine with positively charged

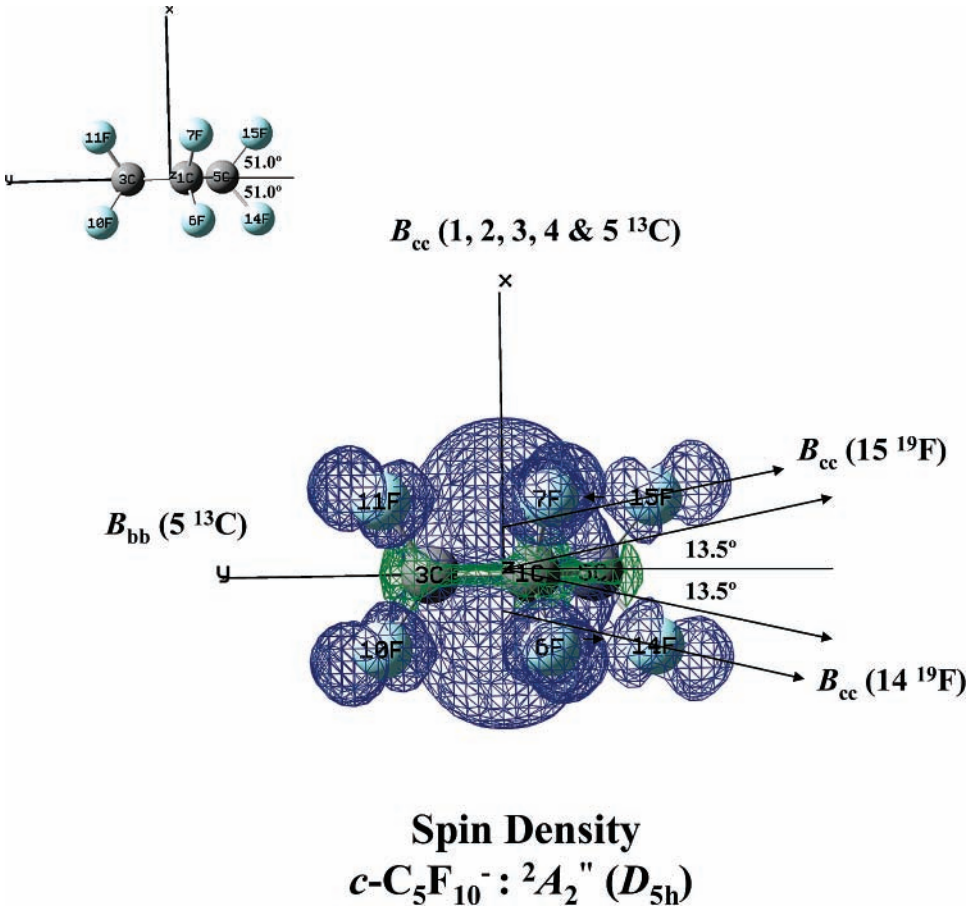

Figure 14. Plots of the SD projected to the $x-y$ plane computed for c-$C_5F_{10}^-$ with the $^2A_2''$(D_{5h}) electronic state. The computations were performed using method C. The principal directions of ^{13}C *hf* splittings at positions 1, 2, 3, 4, and 5 (1^{13}C, 2^{13}C, 3^{13}C, 4^{13}C, and 5^{13}C) and ^{19}F *hf* splittings at positions 14 and 15 (14^{19}F and 15^{19}F) are indicated in the figure. Refer to Figures 7a and 8a for the *x*,*y*,*z* coordinate system and Table 4b for the *hf* principal directions and values.

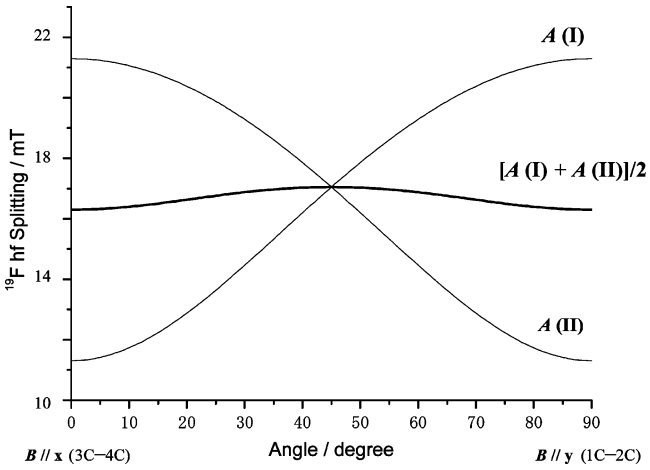

Figure 15. Variation in two different ^{19}F *hf* splittings, *A*(I) and *A*(II), of c-$C_4F_8^-$ in the molecular $x-y$ plane with change in the applied external magnetic field, ***B***, from the *x*-axis to the *y*-axis (refer to Figures 4b, 6, and 12 for the *x*,*y*,*z* system); I and II denote the two diagonally placed sets of four equivalent nuclei ([5F, 6F, 7F, 8F] and [9F, 10F, 11F, 12F], respectively). The bold solid line marked as "[*A*(I) + *A*(II)]/2" corresponds to one-half the sum of two ^{19}F *hf* splittings due to I and II nuclei (one from each set). The ^{19}F *hf* splittings were calculated using the standard formulas[32] from the isotropic and anisotropic *hf* splittings (B_{aa}, B_{bb}, B_{cc}) computed by method C and listed in Table 3. See text for more detail.

species in the matrix, or dissociate to give a perfluorocycloalkyl radical and a fluoride anion. Both of these resonant processes would account for the observed irreversible loss of the c-$C_nF_{2n}^-$ radical anions upon exposure to visible light. However, taking into account both the facts that the lowest calculated excitation energies (>2 eV) are considerably larger than the electron affinities of the studied molecules (0.2−0.8 eV),[12] and the highly delocalized and nonbonding nature of the LUMOs, these being essentially linear combinations of fluorine lone-pair orbitals and, thus, not favoring the breakage of any specific C−F bond, these considerations would indicate electron detachment to be the more-plausible process.

Therefore, it is significant to report direct experimental evidence for photoinduced electron transfer from c-$C_4F_8^-$ to SF_6, with the adiabatic electron affinity of SF_6 (1.05 eV)[33] being greater than that of c-C_4F_8 (0.63 eV).[9,1,12] Figure 17 shows the results when a γ-irradiated TMS solution of both c-C_4F_8 and SF_6 is exposed to visible light at 105 K. Because the concentration of c-C_4F_8 is ca. 40 times higher than that of SF_6, the initial spectrum (a) taken after γ-irradiation and before exposure to visible light is dominated by the lines from c-$C_4F_8^-$, although one can also detect several of the SF_6^- components that are not overlapped by the strong c-$C_4F_8^-$ signals. As shown in the lower spectrum (b), the removal of all the c-$C_4F_8^-$ lines, that takes place upon exposure to visible light, is accompanied by a two-fold increase in the intensity of the SF_6^- spectrum.[19,34] Therefore, this experiment provides direct evidence that the photobleaching of c-$C_4F_8^-$ results in electron transfer from c-$C_4F_8^-$ to SF_6, with the most likely mechanism being electron detachment from c-$C_4F_8^-$ and subsequent recapture by SF_6. Although the quantum yield of this process is difficult to estimate, similar photobleaching experiments that involve a

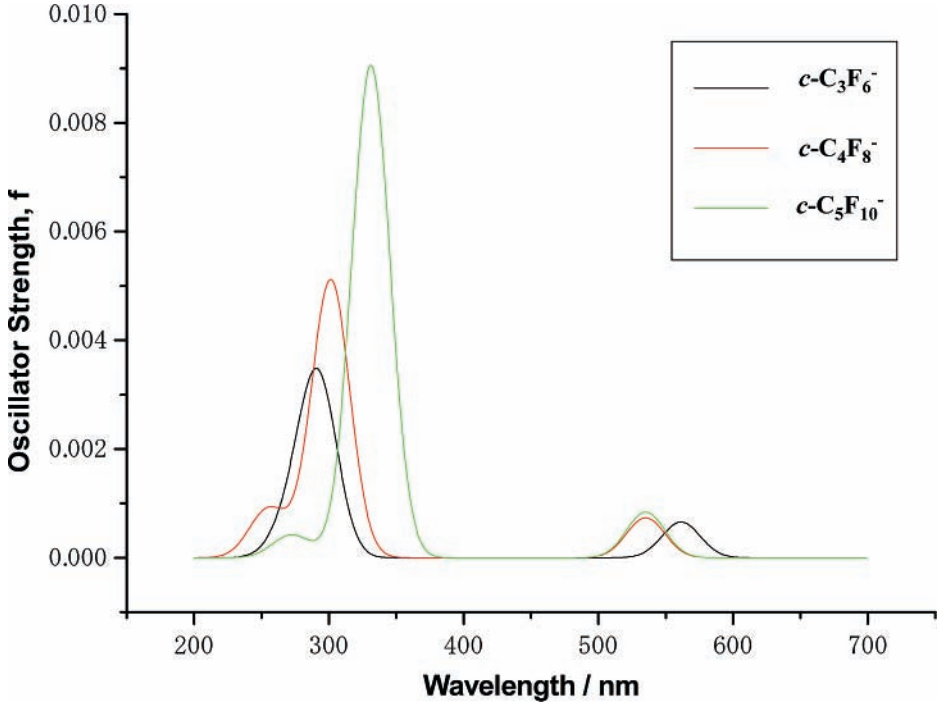

Figure 16. Electronic absorption spectra of c-$C_3F_6^-$ with $^2A_2''$ (D_{3h}) state, c-$C_4F_8^-$ with $^2A_{2u}$ (D_{4h}) state and c-$C_5F_{10}^-$ with $^2A_2''$ (D_{5h}) state computed via a time-dependent (TD) B3LYP density functional theory (DFT) method (6-311+G(d,p) basis set) for the geometries optimized via the UHF/6-311+G(d,p) method. The oscillator strengths (f) are plotted in 200−700 nm range. In the spectral computations, a Gaussian line width of 20 nm was used.

dissociative electron transfer from c-$C_4F_8^-$ to methyl bromide[6] led to a four-fold increase in the CH_3 radical signal.

4. Concluding Remarks

Three perfluorocycloalkane radical anions, c-$C_nF_{2n}^-$ (where $n = 3$, 4, or 5), were generated and stabilized in γ-irradiated tetramethylsilane (TMS) and rigid 2-methyltetrahydrofuran (MTHF) matrices. By recording their temperature-dependent electron spin resonance (ESR) spectra in TMS between 77 K and ca. 170 K, both anisotropic and isotropic features were observed. The isotropic ^{19}F hyperfine (*hf*) splittings observed in the TMS matrix are in excellent agreement with the previous determinations for these radical anions in the neopentane[15,16] and hexamethylethane[13] (HME) matrices. Because these results strongly suggest that matrix effects have a negligible influence on the electronic structure of these radical anions, the experimental ^{19}F *hf* splittings can be compared with the theoretical values that are computed based on the isolated molecule approximation.

This comparison between the experimental and theoretical *hf* couplings for these radical anions previously has been limited only to the isotropic^{19}F *hf* couplings.[13] In the present study, we have performed a series of quantum chemical calculations to further elucidate their geometrical and electronic structures, with particular attention focused on computations of the anisotropic ^{19}F *hf* tensors. These results are suitably compared with the data obtained by analyzing the experimental anisotropic ESR spectra. The unrestricted Hartree−Fock (UHF) computations with 6-311+G(d,p) basis set resulted in planar geometrical structures for the three radical anions: c-$C_3F_6^-$ with $^2A_2''$ (D_{3h} symmetry), c-$C_4F_8^-$ with $^2A_{2u}$ (D_{4h}), and c-$C_5F_{10}^-$ with $^2A_2''$ (D_{5h}) electronic state.

Consistent with previous reports,[4,12a,13] the computations resulted in geometrical structures that are significantly altered by electron attachment. For example, electron attachment to c-C_4F_8 results in a geometrical change from the puckered D_{2d} symmetry to the planar D_{4h} symmetrical structure. This remarkable increase of symmetry on negative ion formation is in sharp contrast to the reduced symmetry in the acyclic perfluorocompounds,[12a] and it is largely attributable to the stabilizing effect resulting from the complete delocalization of the added electron in the planar D_{4h} ring structure. Furthermore, relative to the values in neutral c-C_4F_8,[29] the F−C−F angle decreases by ca. 10° and the C−C bond length decreases by ca. 0.1 Å, while the C−F bond increases by 0.1 Å. This causes an increase of ca. 0.1 Å in the calculated nonbonded F−F distance between neighboring carbons, thereby favoring the reduction in the ring dihedral angle from D_{2d} to D_{4h} symmetry on electron attachment.[4,12a,13] The changes in bond lengths result from the nature of the high-symmetry a_{2u} SOMO with its C−C bonding and C−F antibonding characteristics. Similar changes in bond lengths are observed to occur upon electron attachment to c-C_3F_6 and c-C_5F_{10}.

The isotropic ^{19}F *hf* splittings computed by the B3LYP method (6-311+G(2df,p) basis set) for the UHF optimized geometries (method C) are in much closer agreement with the experimental values (within 0.4 %) than those previously obtained by the B3LYP and MP2 methods (3−9 % and 1−5 %, respectively);[13] the present results yielding 19.78 mT (calc) vs 19.8 mT (exp) for c-$C_3F_6^-$, 14.84 mT (calc) vs 14.85 mT (exp) for c-$C_4F_8^-$, and 11.65 mT (calc) vs 11.6 mT (exp) for c-$C_5F_{10}^-$. Therefore, anisotropic ^{19}F *hf* splittings were computed via the same method and gave principal values that are similar to axially symmetric values for the magnetically equivalent ^{19}F atoms; (−4.90 mT, −4.84 mT, 9.75 mT) for c-$C_3F_6^-$, (−3.54 mT, −3.48 mT, 7.02 mT) for c-$C_4F_8^-$, and (−2.62 mT, −2.56 mT, 5.18 mT) for c-$C_5F_{10}^-$. These anisotropic ^{19}F *hf* splittings, together with their direction cosines computed by method C (B3LYP//UHF),[14] were then used to simulate an anisotropic "powder" spectrum of c-$C_nF_{2n}^-$ (for $n = 3$, 4, 5). Because the

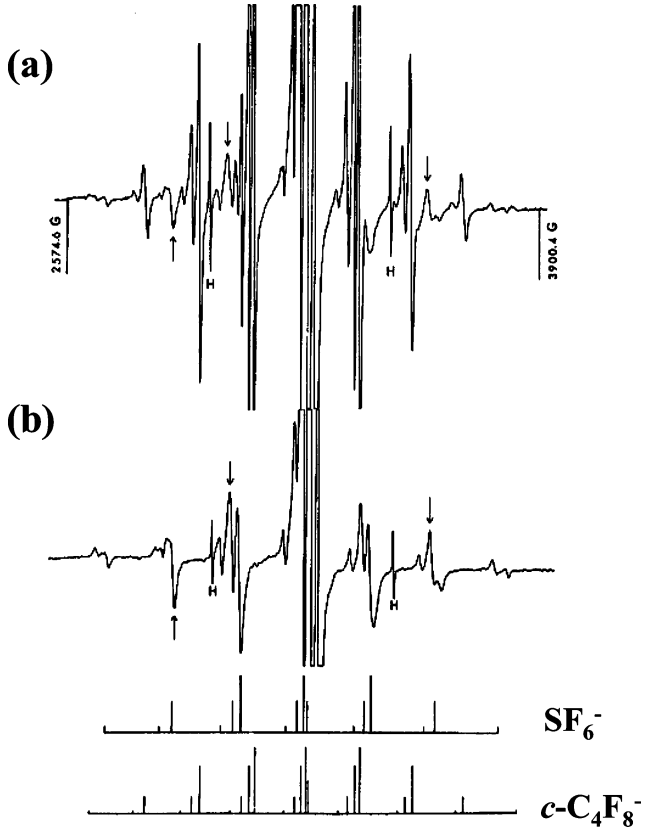

Figure 17. ESR spectra of a γ-irradiated solid solution of 0.03 mol % sulfur hexafluoride (SF_6) and 1.2 mol % *c*-C_4F_8 in TMS at 77 K; the irradiation dose was 5.0 kGy. Spectra (a) and (b) were recorded at 105 K before and after exposing the sample to unfiltered light from a tungsten lamp, respectively. The line diagram shows the expected positions of the second-order ^{19}F *hf* lines for SF_6^- and *c*-$C_4F_8^-$ radical anions calculated from the isotropic ^{19}F *hf* splittings of $a = 19.54$ mT (six ^{19}F nuclei)[19,34] and $a = 14.85$ mT (eight ^{19}F nuclei) listed in Table 1, respectively. (10 G = 1 mT.)

principal values (three parameters) of the ^{19}F *hf* tensor and their directions (three parameters) must be specified for each of the ^{19}F nuclei of the radical anion,[14] this is a much more direct procedure for ESR spectral simulation than the ordinary trial method, which, by necessity, requires a large number of adjustable parameters.

The overall ESR spectral features in the powder spectra of *c*-$C_nF_{2n}^-$ (for $n = 3, 4, 5$) are reproduced quite well by the computations; the error, with respect to the observed total splitting, is within 2.0 % for both *c*-$C_3F_6^-$ and *c*-$C_4F_8^-$. Thus, it follows that the computed anisotropic ^{19}F *hf* coupling tensors must be quite similar to the actual values, paralleling the excellent agreement observed for the isotropic ^{19}F *hf* splittings. In addition, the computed direction cosines of the anisotropic splittings reveal that the maximum (or parallel) ^{19}F anisotropic splittings (B_{cc}) of the six, eight, and ten magnetically equivalent ^{19}F nuclei of *c*-$C_nF_{2n}^-$ (for $n = 3, 4, 5$; D_{nh} structures) are directed out of the molecular plane by angles of $\pm 17.5°$, $\pm 15.4°$, and $\pm 13.5°$ for *c*-$C_3F_6^-$, *c*-$C_4F_8^-$, and *c*-$C_5F_{10}^-$, respectively.

Because of the highly symmetric nature of the a_2'' single occupied molecular orbital (SOMO) (D_{3h}) and a_{2u} SOMO (D_{4h}), identical ^{19}F *hf* splittings are expected for all six and eight ^{19}F nuclei of *c*-$C_3F_6^-$ and *c*-$C_4F_8^-$ along their molecular *z*-axis, i.e., the C_3 and C_4 symmetry axes, respectively. These were evaluated[32] to be 16.7 and 12.4 mT for the ^{19}F nuclei of *c*-$C_3F_6^-$ and *c*-$C_4F_8^-$ from the isotropic and anisotropic *hf* splittings computed by method C. On the other hand, in the carbon ring ($x-y$) plane, symmetry considerations indicate that three different ^{19}F *hf* splittings are expected for *c*-$C_3F_6^-$ with three groups of two ^{19}F nuclei, while two different ^{19}F *hf* splittings apply for *c*-$C_4F_8^-$ with two groups of four nuclei. Although the individual ^{19}F splittings of each group are quite anisotropic, the effective splittings in the $x-y$ plane, which are given by one-third of the sum of three ^{19}F *hf* splittings for *c*-$C_3F_6^-$ and by one-half of the sum of two ^{19}F *hf* splittings for *c*-$C_4F_8^-$, vary only by 0.16 and 0.75 mT, respectively. The relatively small anisotropy in these effective splittings explains the nature of the outermost features observed in the experimental powder spectra. Thus, although only one clearly defined set of wing features is observed for *c*-$C_3F_6^-$, two closely spaced sets are present in the spectrum of *c*-$C_4F_8^-$, which is expected, because of the larger degree of anisotropy.

For the *c*-$C_5F_{10}^-$ radical anion, methods A (B3LYP//B3LYP) and B (B3LYP//MP2) resulted in a C_s geometrical structure with a $^2A'$ ground state. Method B gave an average value of the computed ^{19}F *hf* isotropic splittings, $a(^{19}F) = 11.52$ mT, which is in good agreement with the experimental value of 11.6 mT. Theoretical ESR spectra were simulated for *c*-$C_5F_{10}^-$ using the ^{19}F *hf* tensors computed for both the planar D_{5h} (by method C) and nonplanar C_s (by method B) structures. Although the energies of these two structures differ by as little as ca. 0.15 kcal/mol, only the spectrum calculated for the former structure reproduced the anisotropic experimental spectrum. However, this "static" D_{5h} structure may actually result from a very rapid dynamical averaging of the five possible fluxional C_s structures.

The electronic excitation energies and oscillator strengths were computed for the ground electronic states of *c*-$C_3F_6^-$ ($^2A_2''$ in D_{3h}), *c*-$C_4F_8^-$ ($^2A_{2u}$ in D_{4h}), and *c*-$C_5F_{10}^-$ ($^2A_2''$ in D_{5h}) by time-dependent density functional theory (TD-DFT) methods. The computations resulted in weak oscillator strengths of $f \approx 0.02-0.03$ in a visible range of $\sim 560-530$ nm, which correspond to the electronic transitions from the SOMO to the LUMO of $5a_2'' \Rightarrow 7a_1$ for *c*-$C_3F_6^-$, $5a_{2u} \Rightarrow 6a_{1g}$ for *c*-$C_4F_8^-$, and $6a_2'' \Rightarrow 8a_1$ for *c*-$C_5F_{10}^-$. The prediction of light absorption in the visible region is consistent with the present experimental results, showing that all the ESR spectral lines attributable to the *c*-$C_nF_{2n}^-$ radical anions are removed by exposure of the sample to unfiltered light from a tungsten lamp. In addition, experimental evidence for photoinduced electron transfer from *c*-$C_4F_8^-$ to SF_6 has been obtained by photobleaching experiments in γ-irradiated TMS solutions of both *c*-C_4F_8 and SF_6. Accordingly, these photobleaching studies provide direct evidence that the photoexcited states of these perfluorocyclooalkane anions can undergo simple electron detachment. Photobleaching that results from an alternate decay process by C−F bond dissociation to give a perfluorocycloalkyl radical and a fluoride anion is considered less likely, considering the highly delocalized and nonbonding character of the excess electron in these excited states.

Acknowledgment. This work was supported by the Wenner−Gren Foundation (Sweden) and by the Division of Chemical Sciences, Office of Basic Energy Sciences, United States Department of Energy (under Grant No. DE-FG02-88ER13852). We thank Dr. K. Komaguchi (Hiroshima University) for his help in recording the ESR spectra of *c*-$C_4F_8^-$ in MTHF, Dr. R. I. McNeil for his help in recording the ESR spectra of *c*-$C_4F_8^-$/SF_6^- in TMS, and Dr. P. Persson (Lund University) for his help in the MP2 and TD-DFT computations.

Supporting Information Available: Tables showing complete anisotropic ^{19}F *hf* couplings in a molecular axis system

calculated for *c*-$C_3F_6^-$ with $^2A_2''$ (D_{3h}) electronic state (Table 1), *c*-$C_4F_8^-$ with $^2A_{2u}$ (D_{4h}) electronic state (Table 2), *c*-$C_5F_{10}^-$ with $^2A_2''$ (D_{5h}) electronic state (Table 3), and *c*-$C_5F_{10}^-$ with ^2A(C_s) electronic state (Table 4). Table 5 shows electronic excitation energies and oscillator strengths (*f*) of *c*-$C_3F_6^-$, *c*-$C_4F_8^-$, and *c*-$C_5F_{10}^-$ anions computed via TD-DFT methods. This material is available free of charge via the Internet at http://pubs.acs.org.

References and Notes

(1) (a) Tachi, S. *J. Vac. Sci. Technol. A* **2003**, *21*, S131. (b) Hopwood, J.; Mantei, T. D. *J. Vac. Sci. Technol. A* **2003**, *21*, S139. (c) Teii, S.; Hori, M.; Ito, M.; Goto, T.; Ishii, N. *J. Vac. Sci. Technol. A* **2000**, *18*, 1. (d) Jung, C. O.; Chi, K. K.; Hwang, B. G.; Moon, J. T.; Lee, M. Y.; Lee, J. G. *Thin Solid Films* **1999**, *341*, 112.

(2) Lieberman, M. A.; Lichtenberg, A. J. *Principles of Plasma Discharges and Materials Processing*; Wiley: New York, 1994.

(3) Christophorou, L. G; Mathis, R. A.; James, D. R.; McCorkle, D. L. *J. Phys. D*: *Appl. Phys*. **1981**, *14*, 1889.

(4) Gallup. G. A. *Chem. Phys. Lett.* **2004**, *399*, 206.

(5) (a) Combellas, C.; Kanoufi, F.; Thiebault, A. *J. Phys. Chem. B* **2003**, *107*, 10894. (b) Pud, A. A.; Shapoval, G. S.; Kukhar, V. P.; Mikulina, O. E.; Gervits, L. L. *Electrochim. Acta* **1995**, *40*, 1157. (c) Marsella, J. A.; Gilicinski, A. G.; Coughlin, A. M.; Pez, G. P. *J. Org. Chem.* **1992**, *57*, 2856.

(6) (a) Sprague, E. D.; Williams, F. *J. Chem. Phys.* **1971**, *54*, 5425. (b) Shiotani, M.; Iimura, D.; Murabayashi, S.; Sohma, J. *Int. J. Radiat. Phys. Chem.* **1975**, *7*, 265. (c) Hasegawa, A.; Williams, F. *Chem. Phys. Lett.* **1977**, *46*, 66. (d) Symons, M. C. R. *J. Chem. Res. (S)* **1978**, 360. (e) Wang, J. T.; Williams, F. *J. Am. Chem. Soc.* **1980**, *102*, 2860. (f) Wang, J. T.; Williams, F. *Chem. Phys. Lett.* **1980**, *72*, 557. (g) Sprague, E. D.; Williams, F. *Acc. Chem. Res.* **1982**, *15*, 408. (h) Savéant, J.-M. *Adv. Phys. Org. Chem.* **1990**, *26*, 1. (i) Symons, M. C. R. *Acta. Chem. Scand.* **1997**, *51*, 127. (j) Eberson, L. *Acta Chem. Scand.* **1999**, *53*, 751. (k) Costentin, C.; Robert, M.; Savéant, J.-M. *Chem. Phys.* **2006**, *324*, 40.

(7) Christophorou, L. G.; Olthoff, J. K. *J. Phys. Chem., Ref. Data* **2001**, *30*, 449.

(8) Reinstra-Kiracofe, J. C.; Tschumper, G. S.; Schaefer, H. F., III; Nandi, S.; Ellison, G. B. *Chem. Rev.* **2002**, *102*, 231.

(9) Miller, T. M.; Friedman, J. F.; Viggiano, A. A. *J. Chem. Phys.* **2004**, *120*, 7024.

(10) Miller, T. M.; Morris, R. A.; Miller, A. E. S.; Viggiano, A. A.; Paulson, J. F. *Int. J. Mass Spectrom. Ion Processes* **1994**, *135*, 195.

(11) Hiraoka, K.; Mizuno, T.; Eguchi, D.; Takao, K.; Iino, T.; Yanabe, S. *J. Chem. Phys.* **2002**, *116*, 7574.

(12) (a) Paul, A.; Wannere, C. S.; Kasalova, V.; Schleyer, P. V. R.; Schaefer, H. F., III. *J. Am. Chem. Soc.* **2005**, *127*, 15457. (b) El-Sohly, A. M.; Renault, M. L.; Tschumper, G. S. *J. Phys. Chem. A* **2006**, *110*, 1975.

(13) El-Sohly, A. M.; Tschumper, G. S.; Crocombe, R. A.; Wang, J. T.; Williams, F. *J. Am. Chem. Soc.* **2005**, *127*, 10573.

(14) Shiotani, M.; Persson, P.; Lunell, S.; Lund, A.; Williams, F. *J. Phys. Chem. A* **2006**, *110*, 6307.

(15) Shiotani, M.; Williams, F. *J. Am. Chem. Soc*. **1976**, *98*, 4006.

(16) Hasegawa, A.; Shiotani, M.; Williams, F. *Faraday Discuss. Chem. Soc.* **1977**, *63*, 157.

(17) McNeil, R. I.; Shiotani, M.; Williams, F.; Yim, M. B. *Chem. Phys. Lett.* **1977**, *51*, 438.

(18) McNeil, R. I.; Shiotani, M.; Williams, F.; Yim, M. B. *Chem. Phys. Lett.* **1977**, *51*, 433.

(19) Shiotani, M. In *CRC Handbook of Radiation Chemistry*; Tabata, Y., Ed.; CRC Press: Boca Raton, FL, 1991; pp 544−567.

(20) Atherton, N. M. *Principles of Electron Spin Resonance*; Ellis Horwood: New York, 1993; p 188.

(21) Hasegawa, A.; Hayashi, M.; Kerr, C. M. L.; Williams, F. *J. Mag. Reson.* **1982**, *48*, 192.

(22) Frisch, M. J.; Trucks, G. W.; Schlegel, H. B.; Scuseria, G. E.; Robb, M. A.; Cheeseman, J. R.; Montgomery, J. A., Jr.; Vreven, T.; Kudin, K. N.; Burant, J. C.; Millam, J. M.; Iyengar, S. S.; Tomasi, J.; Barone, V.; Mennucci, B.; Cossi, M.; Scalmani, G.; Rega, N.; Petersson, G. A.; Nakatsuji, H.; Hada, M.; Ehara, M.; Toyota, K.; Fukuda, R.; Hasegawa, J.; Ishida, M.; Nakajima, T.; Honda, Y.; Kitao, O.; Nakai, H.; Klene, M.; Li, X.; Knox, J. E.; Hratchian, H. P.; Cross, J. B.; Bakken, V.; Adamo, C.; Jaramillo, J.; Gomperts, R.; Stratmann, R. E.; Yazyev, O.; Austin, A. J.; Cammi, R.; Pomelli, C.; Ochterski, J. W.; Ayala, P. Y.; Morokuma, K.; Voth, G. A.; Salvador, P.; Dannenberg, J. J.; Zakrzewski, V. G.; Dapprich, S.; Daniels, A. D.; Strain, M. C.; Farkas, O.; Malick, D. K.; Rabuck, A. D.; Raghavachari, K.; Foresman, J. B.; Ortiz, J. V.; Cui, Q.; Baboul, A. G.; Clifford, S.; Cioslowski, J.; Stefanov, B. B.; Liu, G.; Liashenko, A.; Piskorz, P.; Komaromi, I.; Martin, R. L.; Fox, D. J.; Keith, T.; Al-Laham, M. A.; Peng, C. Y.; Nanayakkara, A.; Challacombe, M.; Gill, P. M. W.; Johnson, B.; Chen, W.; Wong, M. W.; Gonzalez, C.; Pople, J. A. et al. *Gaussian 03, Revision B.05*; Gaussian, Inc.: Wallingford, CT, 2004.

(23) Lund, A. *Appl. Magn. Reson.* **2004**, *26*, 365.

(24) Lund A.; Gustafsson, H.; Maruani, J; Shiotani, M. *Spectrochim. Acta A* **2006**, *63*, 830.

(25) Edlund, O.; Lund, A.; Shiotani, M.; Sohma, J.; Thuomas, K. A. *Mol. Phys.* **1976**, *32*, 49.

(26) (a) Maruani, J.; McDowell, C. A.; Nakajima, H.; Raghunatthan, P. *Mol. Phys.* **1968**, *14*, 349. (b) Maruani, J.; Coope, J. A. R.; McDowell, C. A. *Mol. Phys.* **1970**, *18*, 165.

(27) Fessenden, R. W.; Schuler, R. H. *J. Chem. Phys.* **1965**, *43*, 2704.

(28) Li, W.-Z.; Huang, M.-B. *J. Mol. Struct. (THEOCHEM)* **2003**, *636*, 71.

(29) Chiang, J. F.; Bernett, W. A. *Tetrahedron* **1971**, *27*, 975.

(30) (a) Chang, C. H.; Porter, R. F.; Bauer, S. H. *J. Mol. Struct. (THEOCHEM)* **1971**, *7*, 89. (b) Fischer, G.; Purchase, R. L.; Smith, D. M. *J. Mol. Struct. (THEOCHEM)* **1997**, *405*, 159.

(31) Atkins, P., de Paula, J. *ATKINS' Physical Chemistry*, Seventh Edition; Oxford University Press: New York, 2002; p 956.

(32) Weil, J. A.; Bolton, J. R.; Wertz, J. E. *Electron Paramagnetic Resonance*; Wiley: New York, 1994; p 125.

(33) Grimsrud, E. P.; Chowdhury, S.; Kebarle, P. *J. Chem. Phys.* **1985**, *85*, 4989.

(34) (a) Fessenden, R. W.; Schuler, R. H. *J. Chem. Phys.* **1966**, *45*, 1845. (b) Morton, J. R.; Preston, K. F. *Am. Chem. Soc., Symp. Ser*. **1978**, *66*, 386.